JGP Journal of General Physiology

ARTICLE

Acid-sensing ion channel 1a activates IK_{Ca}/SK_{Ca} channels and contributes to endothelium-dependent dilation

Selina M. Garcia[1], Jay S. Naik[1], Thomas C. Resta[1], and Nikki L. Jernigan[1]

Acid-sensing ion channel 1a (ASIC1a) belongs to a novel family of proton-gated cation channels that are permeable to both Na^+ and Ca^{2+}. ASIC1a is expressed in vascular smooth muscle and endothelial cells in a variety of vascular beds, yet little is known regarding the potential impact of ASIC1a to regulate local vascular reactivity. Our previous studies in rat mesenteric arteries suggest ASIC1a does not contribute to agonist-induced vasoconstriction but may mediate a vasodilatory response. The objective of the current study is to determine the role of ASIC1a in systemic vasodilatory responses by testing the hypothesis that the activation of endothelial ASIC1a mediates vasodilation of mesenteric resistance arteries through an endothelium-dependent hyperpolarization (EDH)-related pathway. The selective ASIC1a antagonist psalmotoxin 1 (PcTX1) largely attenuated the sustained vasodilatory response to acetylcholine (ACh) in isolated, pressurized mesenteric resistance arteries and ACh-mediated Ca^{2+} influx in freshly isolated mesenteric endothelial tubes. Similarly, basal tone was enhanced and ACh-induced vasodilation blunted in mesenteric arteries from *Asic1a* knockout mice. ASIC1a colocalizes with intermediate- and small-conductance Ca^{2+}-activated K^+ channels (IK_{Ca} and SK_{Ca}, respectively), and the IK_{Ca}/SK_{Ca}-sensitive component of the ACh-mediated vasodilation was blocked by ASIC1a inhibition. To determine the role of ASIC1a to activate IK_{Ca}/SK_{Ca} channels, we measured whole-cell K^+ currents using the perforated-patch clamp technique in freshly isolated mesenteric endothelial cells. Inhibition of ASIC1a prevented ACh-induced activation of IK_{Ca}/SK_{Ca} channels. The ASIC1 agonist, α/β-MitTx, activated IK_{Ca}/SK_{Ca} channels and induced an IK_{Ca}/SK_{Ca}-dependent vasodilation. Together, the present study demonstrates that ASIC1a couples to IK_{Ca}/SK_{Ca} channels in mesenteric resistance arteries to mediate endothelium-dependent vasodilation.

Introduction

Acid-sensing ion channel 1a (ASIC1a) is a ligand-gated cation channel that belongs to the degenerin/epithelial sodium channel superfamily. There are seven different ASIC subunits (ASIC1a/b, ASIC2a/b, ASIC3, ASIC4, and ASIC5) encoded by five different genes (Waldmann et al., 1997b; Waldmann et al., 1997a; Price et al., 1996; Garcia-Anoveros et al., 1997; Chen et al., 1998; Grunder et al., 2000; Lingueglia et al., 1997; Schaefer et al., 2000). Although ASICs are primarily permeable to Na^+, ASIC1a additionally conducts Ca^{2+}, leading to cell excitability (Xiong et al., 2004; Yermolaieva et al., 2004). ASICs, including ASIC1a, are widely expressed within the central and peripheral nervous systems where they play a role in synaptic plasticity, learning and memory, fear conditioning, nociception, acidosis, mechanosensing, and taste (reviewed in Benarroch, 2014). Despite evidence that ASICs are expressed in vascular smooth muscle and endothelial cells (Grifoni et al., 2008; Jernigan et al., 2009; Chung et al., 2011; Akanji et al., 2019; Lin et al., 2014; Czikora et al., 2017; Garcia et al., 2020; Redd et al., 2021), studies directly assessing the role of vascular ASICs in the regulation of vascular tone are limited, and it remains unclear whether ASICs additionally contribute to cardiovascular homeostasis independent of neural control.

In pulmonary circulation, ASIC1a is mainly expressed in pulmonary arterial smooth muscle cells and contributes to receptor-mediated vasoconstriction and membrane depolarization (Jernigan et al., 2009; Nitta et al., 2014; Jernigan et al., 2021). Despite the expression of ASIC1 in smooth muscle cells of mesenteric resistance arteries, we found that ASIC1 does not contribute to receptor-mediated vasoconstriction in response to endothelin-1 (Garcia et al., 2020). Rather, ASIC1 inhibition tended to augment vasoconstrictor responsiveness at lower concentrations of endothelin-1, suggesting ASIC1 may counteract

[1]Department of Cell Biology and Physiology University of New Mexico School of Medicine, Albuquerque, NM.

Correspondence to Nikki L. Jernigan: njernigan@salud.unm.edu

This work is part of a special issue on Structure and Function of Ion Channels in Native Cells and Macromolecular Complexes.

endothelin-1–induced vasoconstriction. Receptors for endothelin-1 are expressed on both smooth muscle (ET_A and ET_B receptors) and endothelium (ET_B receptors), leading to vasoconstriction and vasodilation, respectively (Clozel et al., 1992). It is therefore possible ASIC1a contributes to endothelium-dependent regulation of vascular tone in small mesenteric arteries.

Although endothelial cells are considered non-excitable cells, an abundance of ion channels are present on the plasma membrane and are integrally involved in endothelial cell function (reviewed in Nilius and Droogmans, 2001). The activation of non-selective ion channels can increase intracellular Ca^{2+} levels, which leads to the production and release of endogenous vasodilators, including nitric oxide (NO) and prostacyclin (PGI_2), as well as eliciting endothelium-dependent hyperpolarization (EDH). In small arteries, particularly in the mesenteric circulation, EDH is the predominant pathway controlling endothelium-dependent vasodilation (Garland and McPherson, 1992; Shimokawa et al., 1996; Brandes et al., 2000). EDH is activated by an increase in endothelial cell Ca^{2+}, which stimulates intermediate- and small-conductance Ca^{2+}-activated K^+ channels (IK_{Ca} and SK_{Ca}, respectively). The spread of hyperpolarizing current from the endothelium to the vascular smooth muscle via myoendothelial gap junctions leads to relaxation of the underlying smooth muscle (reviewed in Garland and Dora, 2017). In the current study, we test the hypothesis that activation of endothelial ASIC1a mediates vasodilation of mesenteric resistance arteries through an EDH-related pathway. To address this hypothesis, we examined the role of ASIC1a in endothelium-dependent vasodilation in isolated-pressurized arteries, Ca^{2+} influx in isolated endothelial tubes, and activation of IK_{Ca} and SK_{Ca} currents via patch-clamp electrophysiology.

Materials and methods

Animals and ethical approval

Studies were completed in adult male Wistar rats (200–250 g body wt, Envigo) or Asic1a knockout (*Asic1a*$^{-/-}$) mice (B6.129-*Asic1*^{tm1Wsh}/J; The Jackson Laboratory; RRID: IMSR_JAX:013733; Wemmie et al., 2002) and age-matched C57BL/6J (The Jackson Laboratory; RRID: IMSR_JAX:000664) wild-type controls (*Asic1a*$^{+/+}$). Homozygotes and/or heterozygotes were bred and the disruption of *Asic1a* gene was confirmed by PCR and agarose gel electrophoresis using a three-primer system to detect both wild-type and disrupted alleles: 5′-CATGTCACCAAGCTCGAC GAGGTG-3′ (*Asic1a*$^{+/+}$ forward primer), 5′-TGGATGTGGAAT GTGTGCGA-3′ (*Asic1a*$^{-/-}$ forward primer), 5′-CCGCCTTGAGCG GCAGGTTTAAAGG-3′ (*Asic1a*$^{+/+}$and *Asic1a*$^{-/-}$ reverse primer). Animals were housed in polyacrylic cages (one to three per cage) in a specific pathogen-free animal care facility and maintained on a 12:12 h light–dark cycle. Animals were supplied with clean bedding and polycarbonate rodent tunnels and other items for environmental enrichment. Water and standard chow (Teklad soy protein-free diet no. 2920; Envigo) were provided ad libitum. All animals were anesthetized with an overdose of pentobarbital sodium (200 mg/kg, i.p.) and immediately euthanized by exsanguination after the loss of consciousness. All protocols used in this study were reviewed and approved by the Institutional Animal Care and Use Committee of the University of New Mexico School of Medicine (#19-200899-HSC Protocol) and abide by the National Institutes of Health guidelines for animal use.

Immunofluorescence in mesenteric resistance arteries

Tissue sections (5 µm thick) were prepared from paraffin-embedded mesentery tissue from Wistar rats and mounted onto Superfrost Plus slides (Thermo Fisher Scientific). Antibody–antigen binding was enhanced by a heat-mediated antigen retrieval method in which sections were held at 95°C for 15 min in a 10 mM Na^+-citrate buffer (pH 6.0) containing 0.05% Tween 20. Sections were incubated with primary (48 h at 4°C) and secondary antibodies (24 h at 4°C), as indicated in Table 1. We have previously determined the specificity of goat anti-ASIC1 using wild-type and knockout mice (Nitta et al., 2014). Sections were mounted with FluoroGel (Electron Microscopy Sciences), and images were acquired sequentially by confocal microscopy (TCS SP5; Leica) using Argon (488 nm/~20 mW), HeNe (543 nm/~1 mW), and HeNe (633 nm/~10 mW) class IIIb lasers and a 63×/1.3 glycerol objective.

To visualize the internal elastic lamina (IEL), pressurized mesenteric resistance arteries were fixed with 4% paraformaldehyde for 20 min and permeabilized with 0.2% Triton-X. Arteries were incubated with rabbit anti-ASIC1 and secondary antibodies as indicated in Table 1. Arteries were whole mounted with Prolong Gold (P10144; Thermo Fisher Scientific), and 3-D (xyz) images of the vessel wall were acquired by confocal microscopy (TCS-SP8; Leica) in line sequential mode at 200 Hz using a 63×/1.4 NA oil objective with a pinhole of 1 AU (0.896 nm optical section). Sampling rates (voxel dimensions) within the 1,024 × 1,024 formatted image were 80 nm for xy and 180 nm for z intervals. A pulsed, white-light laser was set at 488 nm (3%) to detect ASIC1 immunofluorescence emissions at 510–520 nm. Intrinsic IEL autofluorescence emissions from 602 to 622 nm were also collected to determine spatial boundaries using the white-light laser set at 554 nm (3%). All images in the z-stack were postprocessed by deconvolution (Huygen's Essential, Scientific Volume Imaging) as described elsewhere (Noureddine et al., 2021).

Pressure myography in mesenteric resistance arteries

Small mesenteric arteries from rats or mice were cannulated and pressurized for dimensional analysis as previously described (Garcia et al., 2020). Briefly, animals were anesthetized with pentobarbital sodium (200 mg/kg, i.p.) and the mesentery was removed and immediately placed in PSS (in mM: 130 NaCl, 4 KCl, 1.2 $MgSO_4$, 4 $NaHCO_3$, 1.8 $CaCl_2$, 10 HEPES, 1.18 KH_2PO_4, and 6 glucose; pH adjusted to 7.4 with NaOH). Third- to fourth-order mesenteric arteries (100–200 µm inner diameter [ID]) of ~1 mm in length and without visible side branches were dissected free and transferred to a vessel chamber (CH-1, Living Systems). The proximal end of the artery was cannulated with a tapered glass pipette, secured in place with a single strand of silk ligature, and gently flushed to remove blood from the lumen. The vessel was stretched longitudinally to approximate in situ length and

Table 1. **List of primary and secondary antibodies used for immunofluorescence**

Antibody	Company, Cat. #	RRID	Host; clone	Dilution	Fig. #	Reference
Primary						
CD31	Abcam, ab124432	AB_2802125	Rabbit; poly	1:250	Fig. 1	
αSMA	Sigma-Aldrich, A2547	AB_476701	Mouse; mono	1:300	Fig. 1	
ASIC1 (E–15)	Santa Cruz Biotechnology, sc-13903	AB_633515	Goat; poly	1:50	Figs. 1, 5, and 6	Nitta et al., 2014
ASIC1	Millipore Sigma, AB5674P	AB_91972	Rabbit; poly	1:100	Fig. 6 E	Jernigan et al., 2009
STIM1 (44/GOK)	BD Biosciences, 610954	AB_398267	Mouse; mono	1:200	Fig. 5	Krishnan et al., 2022
IK1 (D-5)	Santa Cruz Biotechnology, sc-365265	AB_10841432	Mouse; mono	1:50	Fig. 6	Lu et al., 2017
KCNN3 ($K_{Ca}2.3$)	Alomone Labs, APC-025	AB_10613112	Rabbit; poly	1:200	Fig. 6	Kim et al., 2012
Secondary						
Alexa Fluor 488 anti-rabbit IgG (H + L)	Jackson ImmunoResearch Laboratories, Inc 711-546-152	AB_2340619	Donkey; poly	1:500	Fig. 1	
Cy3 AffiniPure anti-goat IgG (H + L)	Jackson ImmunoResearch Laboratories, Inc 705-165-147	AB_2307351	Donkey; poly	1:500	Figs. 1 and 5 C	
Alexa Fluor 647 anti-mouse IgG (H + L)	Jackson ImmunoResearch Laboratories, Inc 715-605-150	AB_2340862	Donkey; poly	1:500	Figs. 1 and 5 C	
Alexa Fluor 647 anti-rabbit IgG (H + L)	Jackson ImmunoResearch Laboratories, Inc 711-605-152	AB_2492288	Donkey; poly	1:500	Fig. 5 D	

pressurized with a servo-controlled peristaltic pump (Living Systems) to 75 mm Hg. Arteries were required to hold pressure when switching off the servo-control function to verify the absence of leaks; any vessel with apparent leaks was discarded. The vessel chamber was superfused with PSS at 5 ml/min at 37°C. Images were obtained using an Eclipse TS100 microscope (Nikon) and IonOptix CCD100M camera to measure ID, and dimensional analysis was performed by IonOptix Ion Wizard software (IonOptix).

Arteries were incubated at room temperature with PSS containing the cell-permeable ratiometric Ca^{2+}-sensitive fluorescent dye fura-2 acetoxymethyl ester (fura-2 AM, 2 µM; F1201; Life Technologies) and 0.02% pluronic acid (P3000MP; Life Technologies) for 45 min, as previously described (Garcia et al., 2020). Fura-2-loaded vessels were alternately excited at 340 and 380 nm at a frequency of 1 Hz with an IonOptix Hyperswitch dual-excitation light source, and the respective 510-nm emissions were collected with a photomultiplier tube. After subtracting background fluorescence, emission ratios (F_{340}/F_{380}) were calculated with Ion Wizard software (IonOptix) and recorded continuously throughout the experiment as an index of vessel wall intracellular Ca^{2+} concentration ($[Ca^{2+}]_i$).

Rat mesenteric artery vasoreactivity

Vasoconstrictor reactivity and changes in vessel wall $[Ca^{2+}]_i$ to the α_1-adrenergic agonist phenylephrine (PE; Sigma-Aldrich) was assessed by superfusion (5 ml/min at 37°C) of cumulative concentrations of PE (10^{-8} to 10^{-5} M) in isolated rat mesenteric arteries. To assess vasodilatory responses, arteries were first preconstricted (~30–50%) with the thromboxane A_2 analog, U-46619 (Cayman Chemical), before the superfusion of cumulative concentrations of the muscarinic receptor agonist, ACh (10^{-9} to 10^{-5} M; Sigma-Aldrich) or arachidonic acid (AA; 10^{-8} to 10^{-5} M; Cayman Chemical). To determine the contribution of ASIC1a to PE vasoconstrictor and ACh vasodilatory responses, arteries were pretreated (lumen and bath) with the specific ASIC1a antagonist, psalmotoxin 1 (PcTX1, 20 nM; Phoenix Peptides). To assess vasodilation to the ASIC1 agonist, α/β-MitTx, isolated mesenteric arteries were luminally perfused at a rate of 50 µl/min with a bolus of α/β-MitTx (200 nM). In separate experiments, vasodilatory responses were determined in arteries following pretreatment with the NO synthase inhibitor, Nω-nitro-L-arginine (L-NNA; 100 µM; Sigma-Aldrich); cyclooxygenase inhibitor, indomethacin (10 µM; Sigma-Aldrich); or the IK_{Ca} channel antagonist, Tram-34 (1 µM; Tocris Bioscience); and the SK_{Ca} antagonist, Apamin (100 µM; Tocris Bioscience) as described previously (Naik and Walker, 2018).

Mouse mesenteric artery vasoreactivity

Due to rapid desensitization and tachyphylaxis, a bolus dose of angiotensin II (10^{-7} M) and ACh (10^{-6} M) was used to determine vasoconstrictor and vasodilatory responses in mouse mesenteric arteries instead of dose-response curves. For ACh-induced dilation, arteries were first preconstricted (~30–50%) with the thromboxane A_2 analog, U-46619.

Freshly isolated mesenteric endothelial tubes

Mesenteric endothelial tubes were freshly isolated as previously described (Naik et al., 2016). Third- and fourth-order arteries

were dissected and cut into small pieces in HEPES-based PSS buffer containing 1% bovine serum albumin (BSA) and sodium nitroprusside (10^{-5} M). Arterial segments were then enzymatically digested in PSS containing 0.15% BSA, papain (13 U/ml; Sigma-Aldrich), collagenase type 2 (427 U/ml; Worthington Biochemical), and dithiothreitol (1 mg/ml; Sigma-Aldrich) for 40 min at 37°C. Arteries were gently triturated using a glass fire-polished micropipette, secured in the vessel chamber, and incubated in PSS containing fura-2 AM (2 µM; Life Technologies) and pluronic acid (0.05%; Life Technologies) for 30 min at 32°C.

Endothelial Ca^{2+} entry

Mn^{2+} was used as a Ca^{2+} surrogate to determine Ca^{2+} influx in fura-2-loaded mesenteric endothelial tubes. Mn^{2+} binds and quenches fura-2 fluorescence. Percent quenching was monitored at the Ca^{2+} isosbestic wavelength (360 nm) of fura-2 at a frequency of 1 Hz with an IonOptix Hyperswitch dual excitation light source (IonOptix), and the respective 510 nm emissions were detected with a photomultiplier tube as previously described (Jernigan et al., 2009; Paffett et al., 2007). Endothelial Ca^{2+} influx was determined by superfusion (5 ml/min at 37°C) with $MnCl_2$ (500 µM) in Ca^{2+}-free PSS in the absence (time control) or presence of ACh (10^{-5} M) or the protein kinase C (PKC) activator, phorbol 12-myristate 13-acetate (PMA, 10 µM; Cayman Chemical). Experiments were additionally conducted in the absence and presence of the ASIC1 antagonist, PcTX1 (20 nM), or the phospholipase A_2 (PLA_2) antagonist, methyl arachidonyl fluorophosphonate (MAF, 5 µM; Cayman Chemical). To assess store-operated Ca^{2+} entry (SOCE), endothelial tubes were superfused with Ca^{2+}-free PSS (without EGTA) containing cyclopiazonic acid (CPA, 10 µM) for 15 min. $MnCl_2$ (500 µM) was added to the superfusate for 10 min. Parallel experiments were performed in the presence of PcTX1. Mn^{2+} quenching of fura-2 fluorescence was calculated as the percentage change in fluorescence intensity (F) from baseline fluorescence intensity at time 0 (F_0).

Colocalization by immunofluorescence and proximity ligation assay

Freshly isolated endothelial tubes were placed on Superfrost Plus slides (Thermo Fisher Scientific) and fixed with 2% paraformaldehyde. For immunofluorescence, mesenteric endothelial tubes were incubated with primary and secondary antibodies as described in Table 1. For the proximity ligation assay (PLA), endothelial tubes were incubated with Duolink blocking buffer for 30 min at 37°C and then incubated overnight with primary antibodies as indicated in Table 1. Cells were then incubated with anti-rabbit PLUS and anti-mouse MINUS probes (1:5) for 1 h at 37°C. The omission of one or both primary antibodies served as the negative control. Samples were amplified with Duolink In Situ Detection Reagent Orange (excitation/emission: 554/579 nm; Sigma-Aldrich) for 100 min at 37°C. Endothelial nuclei were stained with Sytox Green nucleic acid stain (1: 10,000; #S7020; Invitrogen). Endothelial tubes were mounted with FluoroGel (Electron Microscopy Sciences), and the images were acquired sequentially with a 63×/1.3 glycerol objective by confocal microscopy (TCS SP5; Leica) using Argon (488 nm/~20 mW), HeNe (543 nm/~1 mW), and HeNe (633 nm/~10 mW) class IIIb lasers to determine colocalization.

Isolation of mesenteric endothelial cells and patch clamp electrophysiology

Mesenteric arteries (third to fifth order) were placed in a dissociation buffer containing (in mM) 55 NaCl, 80 Na-glutamate, 6 KCl, 2 $MgCl_2$, 0.1 $CaCl_2$, 10 glucose, and 10 HEPES; pH was adjusted to 7.3 with NaOH as described previously (Ottolini et al., 2020). Endothelial cells were enzymatically dissociated with 1 mg/ml neutral protease (LS02100; Worthington Biochemicals) and 1 mg/ml elastase (LS002290; Worthington Biochemicals) for 1 h at 37°C followed by additional 5 min with 1.5 mg/ml collagenase II (4174; Worthington Biochemicals). Single endothelial cells were dispersed by gentle trituration with a fire-polished pipette in Ca^{2+}-free PSS and were positively identified as endothelial cells following a 30-min incubation with Lycopersicon Esculentum (Tomato) Lectin, Dylight 594 (1:1,000; DL-1177; Vector Laboratories).

K^+ current recordings were performed in freshly dispersed endothelial cells at room temperature (~23°C) using a perforated, whole-cell patch-clamp configuration in voltage-clamp mode. The extracellular solution consisted of (in mM) 140 NaCl, 4 KCl, 2 $CaCl_2$, 1 $MgCl_2$, 10 HEPES, and 10 glucose; pH was adjusted to 7.4 with NaOH. Patch electrodes were pulled from borosilicate filamented glass (#BF-150-86-10; Sutter Instruments) with a micropipette puller (P-87; Sutter Instruments) and fire-polished with a microforge (MF-830; Narishige) to achieve a pipette resistance of 3–6 MΩ. The pipette solution contained (in mM) 110 K-aspartate, 30 KCl, 10 NaCl, 1 $MgCl_2$, 0.003 $CaCl_2$, and 10 HEPES; pH was adjusted to 7.2 with KOH. The osmolarity of all solutions was adjusted to ~290 (pipette) and ~300 (extracellular) mOsm/liter with sucrose. β-Escin (E1378; Sigma-Aldrich) was used as the perforating agent and was dissolved in the pipette solution to reach a final concentration of 25 µM. Patch electrodes were controlled by a motorized micromanipulator (MP-225; Sutter Instruments). After achieving a seal resistance of >1 GΩ and a series resistance <25 MΩ, whole-cell K^+ currents were generated with an Axopatch 200B amplifier (Axon Instruments) and measured in response to voltage steps applied from −140 to +100 mV in 20-mV increments from a holding potential of −50 mV. Currents were filtered with a lowpass Bessel filter at 1 kHz, digitized (1440A Digitizer; Molecular Devices), and recorded using pClamp software (Molecular Devices). Currents were normalized to cell capacitance to obtain current density (pA/pF), and current–voltage (I-V) relationships were generated from the last 50 ms of each stimulus.

Calculations and statistics

All data are expressed as means ± SE. Values of *n* are biological replicates and refer to the number of animals in each group. Statistical comparisons were made using Prism 9 (GraphPad Software). The statistical tests used are reported in the figure legends. A probability of <0.05 with a power level of 0.80 was accepted as statistically significant for all comparisons.

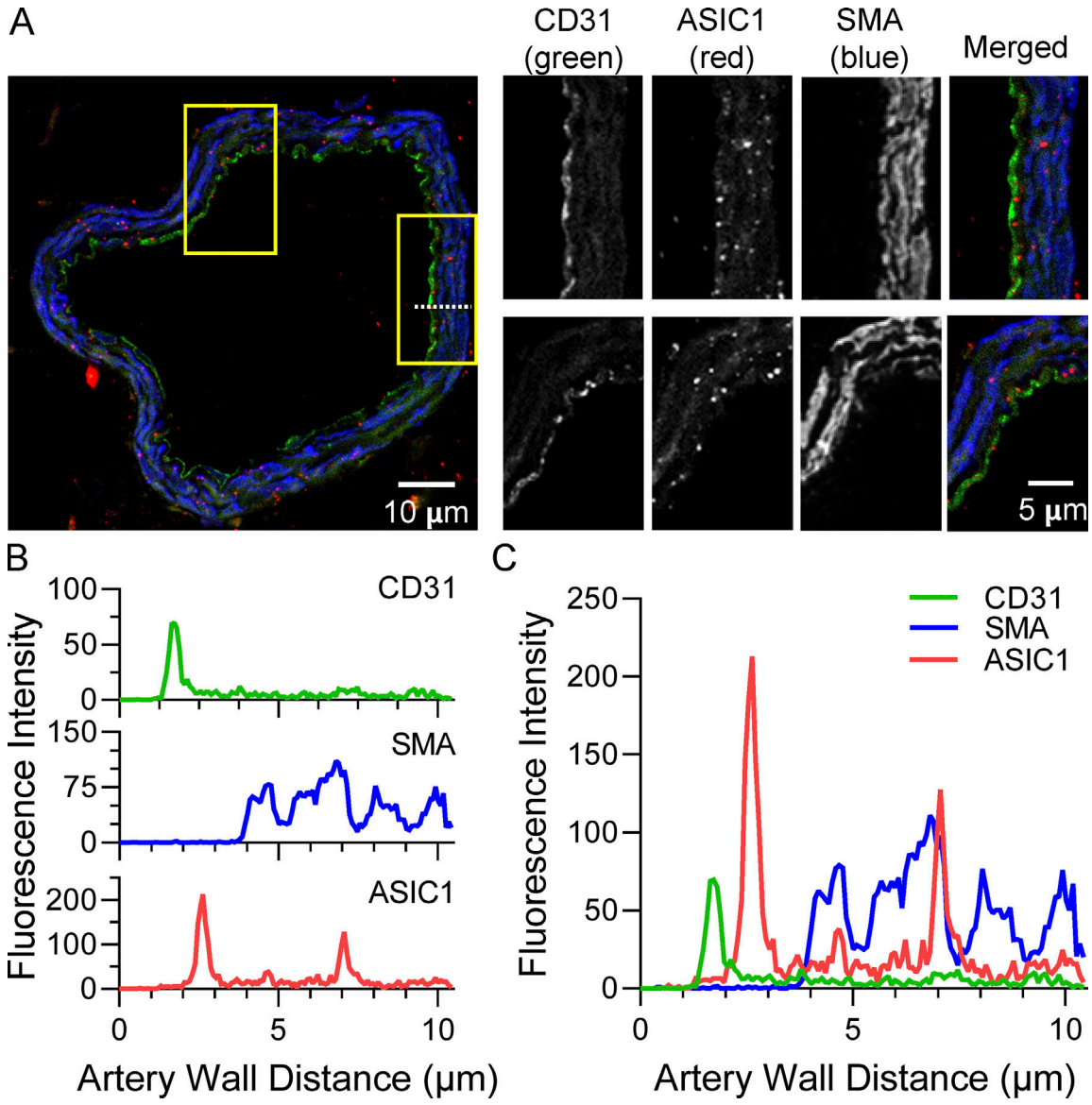

Figure 1. **ASIC1 is expressed in mesenteric vascular smooth muscle and endothelial cells. (A)** Cross-section of a mesenteric artery showing immunofluorescence of the endothelial marker, CD31 (green), ASIC1 (red), and smooth muscle α-actin (blue). Yellow rectangles represent zoomed-in images to the right. **(B and C)** The fluorescence intensity profile across the dotted white line shown in A for both individual (B) and merged (C) fluorescence intensity of CD31, SMA, and ASIC1.

Results

ASIC1 inhibition attenuates ACh-induced dilation in mesenteric arteries

ASIC1 immunoreactivity was detected as punctate fluorescence within both the endothelial and smooth muscle cell layers of mesenteric arteries (Fig. 1). Inhibition of ASIC1 with PcTX1 did not significantly alter basal inner diameter (vehicle: 170 ± 7 µm and PcTX1: 169 ± 5 µm; n = 13/14; P = 0.8754) but did augment basal vessel wall $[Ca^{2+}]_i$ (Fig. 2 A) in rat mesenteric arteries. Although PcTX1 did not significantly alter PE-induced vasoconstrictor responses (Fig. 2 B) or changes in the vessel wall $[Ca^{2+}]_i$ (Fig. 2 C), ACh-induced endothelium-dependent vasodilatory responses were significantly attenuated in the presence of PcTX1 (Fig. 2, D–F). Interestingly, PcTX1-treated mesenteric arteries tended to reach similar peak vasodilatory responses to ACh as vehicle-treated arteries (Fig. 2, D and E). However, the vasodilatory responses in the presence of PcTX1 were more transient, and the sustained vasodilatory response to ACh was largely attenuated compared with vehicle-treated arteries (Fig. 2, D and F).

Passive vessel ID was similar between *Asic1a*$^{+/+}$ and *Asic1a*$^{-/-}$ mice (187 ± 10 and 191 ± 8 µm, respectively; n = 12; P = 0.7888); however, both basal tone (Fig. 3 A) and basal vessel wall $[Ca^{2+}]_i$ (Fig. 3 B) were significantly augmented in mesenteric arteries from *Asic1a*$^{-/-}$ mice. Similar to the pharmacological inhibition of ASIC1 in rats, Ang II-induced vasoconstrictor responses (Fig. 3 C) and changes in vessel wall $[Ca^{2+}]_i$ (Fig. 3 D) in mesenteric arteries were not significantly affected by genetic deletion of

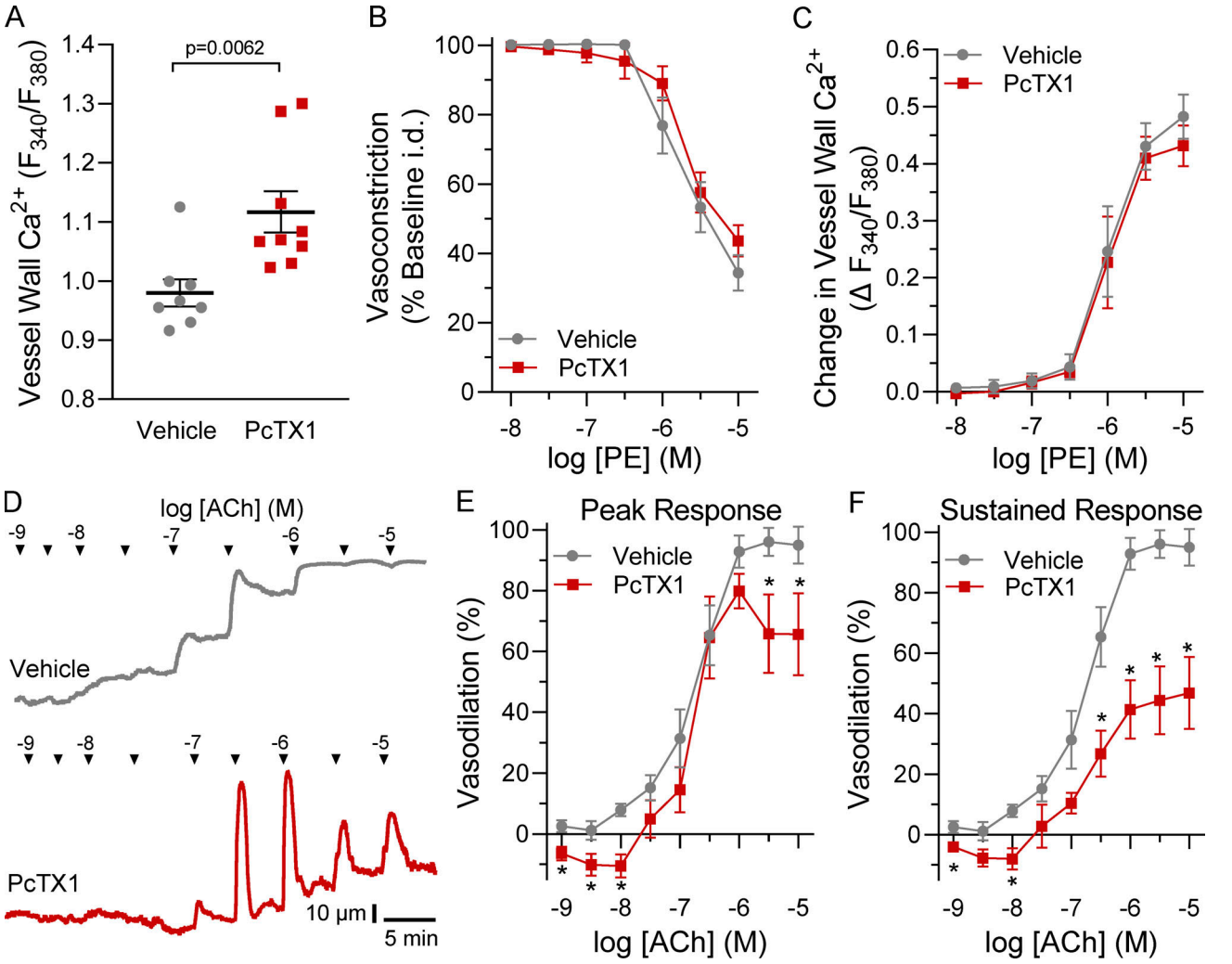

Figure 2. **ASIC1a contributes to ACh-induced vasodilation in mesenteric arteries. (A)** Basal vessel wall intracellular $[Ca^{2+}]$ (F_{340}/F_{380}) in mesenteric arteries in the presence of vehicle or PcTX1 (20 nM). **(B and C)** Vasoconstriction (percent baseline inner diameter; B) and changes in vessel wall $[Ca^{2+}]$ ($\Delta F_{340}/F_{380}$) in response to PE (10^{-8} to 10^{-5} M; C) in the presence of vehicle or PcTX1. **(D)** Representative traces showing changes in vessel inner diameter (µm) in response to increasing doses of ACh (10^{-9} to 10^{-5} M) in preconstricted mesenteric arteries. **(E and F)** The percent peak (E) and sustained (F) vasodilatory responses to ACh in the presence or absence of PcTX1. *n* = 5–6 animals (biological replicates)/group, analyzed by unpaired *t* tests, *P < 0.05 vs. vehicle. P values for data in E from 10^{-9} to 10^{-5} M ACh are 0.0158, 0.0384, 0.0017, 0.1907, 0.2096, 0.9620, 0.1264, 0.0415, and 0.0430. P values for data in F from 10^{-9} to 10^{-5} M ACh are 0.0269, 0.0661, 0.0031, 0.1524, 0.0884, 0.0151, 0.0008, 0.0014, and 0.0041.

Asic1a. However, both peak (Fig. 3, E and F) and sustained (Fig. 3, E and G) ACh-induced vasodilatory responses were significantly blunted in mesenteric arteries from *Asic1a*$^{-/-}$ mice. Together, these observations demonstrate ASIC1's involvement in ACh-induced mesenteric vasodilation.

ASIC1 contributes to ACh-induced endothelial Ca^{2+} influx

To specifically examine the role of ASIC1 in endothelial Ca^{2+} influx, we (1) used freshly isolated mesenteric endothelial tubes (Fig. 4 A) to eliminate influences from the smooth muscle layer and (2) used the Mn^{2+}-quenching technique, which allows for the determination of Ca^{2+} influx independent of concurrent Ca^{2+} release, sequestration, or efflux. Passive Mn^{2+} influx in non-stimulated endothelial tubes due to basal activity of constitutively active cation channels accounts for ~20% quenching of fura-2 fluorescence (Fig. 4, B and C). The addition of ACh significantly increased the quenching of fura-2 fluorescence that was largely inhibited by the ASIC1 antagonist, PcTX1. There was no significant difference between basal levels and ACh + PcTX1 (P = 0.1385). These data indicate that ASIC1 facilitates ACh-induced Ca^{2+} entry in mesenteric endothelial cells.

PKC activates ASIC1 in mesenteric endothelial tubes

To assess the molecular mechanism(s) by which ACh activates ASIC1, we first examined SOCE as ASIC1 is activated by store depletion in pulmonary arterial smooth muscle cells (Jernigan et al., 2009; Garcia et al., 2020). Stromal interaction molecule 1 (STIM1) is the key molecule involved in sensing the levels of Ca^{2+} in the sarcoplasmic reticulum (Liou et al., 2005; Roos et al., 2005). Upon store depletion, STIM1 undergoes a conformational

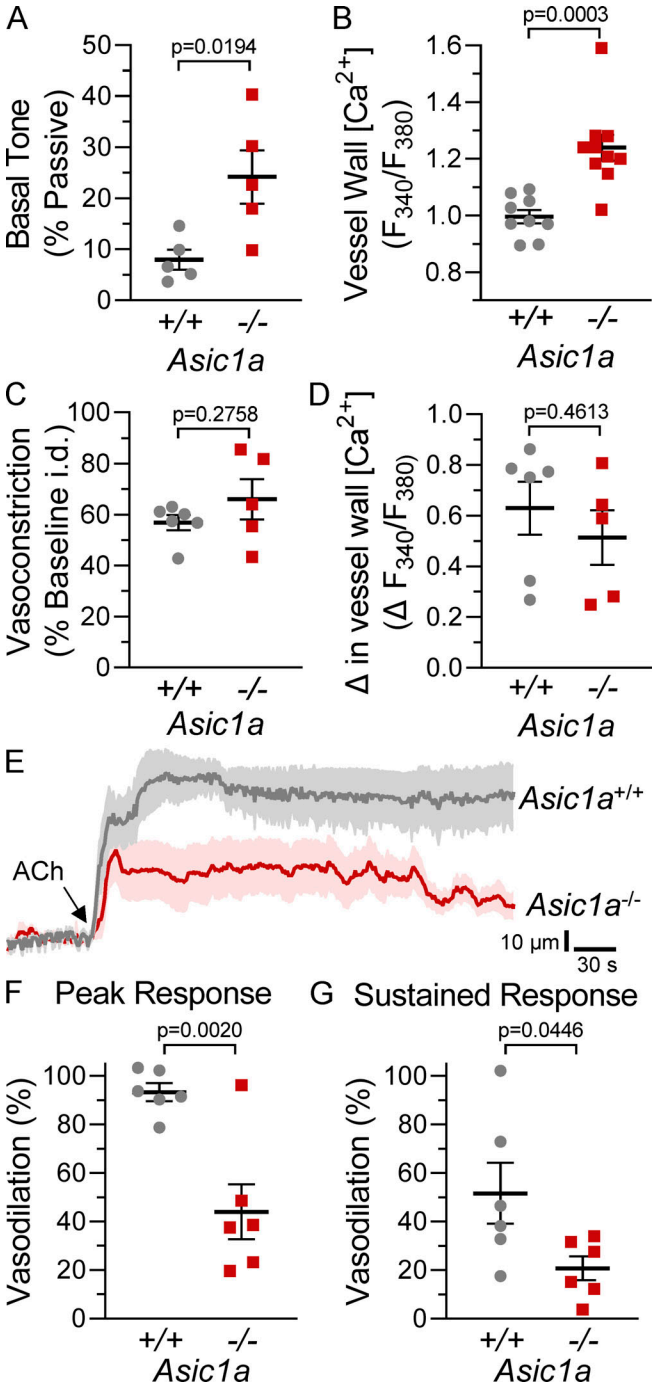

Figure 3. **Augmented basal tone and blunted ACh-induced vasodilation in mesenteric arteries from *Asic1a*$^{-/-}$ mice. (A and B)** Basal tone (percent passive diameter; A) and basal vessel wall intracellular [Ca^{2+}] (F_{340}/F_{380}; B) in mesenteric arteries from *Asic1a*$^{+/+}$ or *Asic1a*$^{-/-}$ mice. **(C and D)** Vasoconstriction (percent baseline inner diameter; C) and changes in the vessel wall [Ca^{2+}] (Δ F_{340}/F_{380}; D) in response to Ang II (10^{-7} M). **(E)** Averaged traces showing changes in vessel inner diameter (µm) in response to ACh (10^{-6} M) in preconstricted mesenteric arteries from *Asic1a*$^{+/+}$ or *Asic1a*$^{-/-}$ mice. **(F and G)** Summary data showing percent peak (F) and sustained (G) vasodilatory responses to ACh. Biological replicates were analyzed by unpaired *t* tests.

change, multimerizes, and translocates to regions of the sarcoplasmic reticulum adjacent to the plasma membrane where subsequent binding of STIM1 to Ca^{2+}-permeable channels triggers the influx of Ca^{2+} across the plasma membrane. Although both ASIC1 and STIM1 are present in the mesenteric endothelium (Fig. 5 A), they did not colocalize, as evidenced by the lack of a positive Duolink proximity ligation interaction (Fig. 5 B). It is worth noting that we have previously shown a positive interaction between ASIC1 and STIM1 in vascular smooth muscle, suggesting this antibody combination can elicit a PLA response (Garcia et al., 2020). Consistent with a lack of ASIC1–STIM1 interaction, PcTX1 did not affect SOCE in mesenteric endothelial tubes (Fig. 5, C and D). We next assessed the possibility that ACh activates ASIC1 through AA since AA is known to stimulate ASIC1 in rat sensory neurons (Smith et al., 2007). Although inhibition of PLA_2 with MAF had a similar effect as PcTX1 to reduce ACh-induced fura-2 quenching (Fig. 5 E), there was an additive effect of MAF and PcTX1, suggesting separate pathways are involved. To further assess this possibility, we examined the effect of PcTX1 on AA-induced vasodilation and found that PcTX1 did not significantly alter AA-induced dilation (Fig. 5 F). ASIC1 can also be regulated by PKC (Bashari et al., 2009; Berdiev et al., 2002; Xiong et al., 2013; Herbert et al., 2016), and we found that PcTX1 largely blunted PMA-induced fura-2 Mn^{2+} quenching (Fig. 5 G), suggesting ASIC1 may be activated by ACh secondary to PKC activation.

ASIC1 contributes to EDH-mediated vasodilation

An increase in endothelial Ca^{2+} influx induces relaxation of the underlying smooth muscle through varying contributions of NO, PGI_2, and EDH. To determine the EDH component of ACh-induced vasodilation in small mesenteric arteries, we used L-NNA and indomethacin to inhibit NO synthase and cyclooxygenase, respectively (Fig. 6 A). Approximately 60% of the ACh-induced vasodilatory response is EDH-dependent. IK_{Ca} and SK_{Ca} channels have a prominent role in this response as inhibition of these channels with Tram-34/Apamin prevents EDH-mediated vasodilation (Fig. 6 A and Table 2). Inhibition of ASIC1 with PcTX1 similarly abolished this EDH-mediated vasodilatory response (Fig. 6 A and Table 2). Since there was not a significant change in inner diameter in response to ACh in the presence of PcTX1 or TRAM-34/Apamin (Table 2), we were unable to assess the potential additive effects of combining these drugs. These data indicate ASIC1 may be involved in the same vasodilatory pathway as IK_{Ca} and SK_{Ca}.

ASIC1 Colocalizes with IK_{Ca} and SK_{Ca}

Immunofluorescence in freshly dispersed endothelial tubes reveals the relative expression and colocalization of ASIC1 with IK_{Ca} and SK_{Ca}. IK_{Ca} (Fig. 6 B) and SK_{Ca} (Fig. 6 C) are diffusely distributed along the cell membrane. ASIC1 immunofluorescence is punctate and interspersed within IK_{Ca} and SK_{Ca} immunofluorescence. Using a Duolink PLA, we identified a positive PLA signal along the cell membrane suggesting ASIC1 is located in close proximity to both IK_{Ca} and SK_{Ca} channels in endothelial tubes (Fig. 6 D). There was no significant difference in the number of puncta per cell (ASIC1-IK_{Ca} 9 ± 3; ASIC1-SK_{Ca}: 8 ± 3;

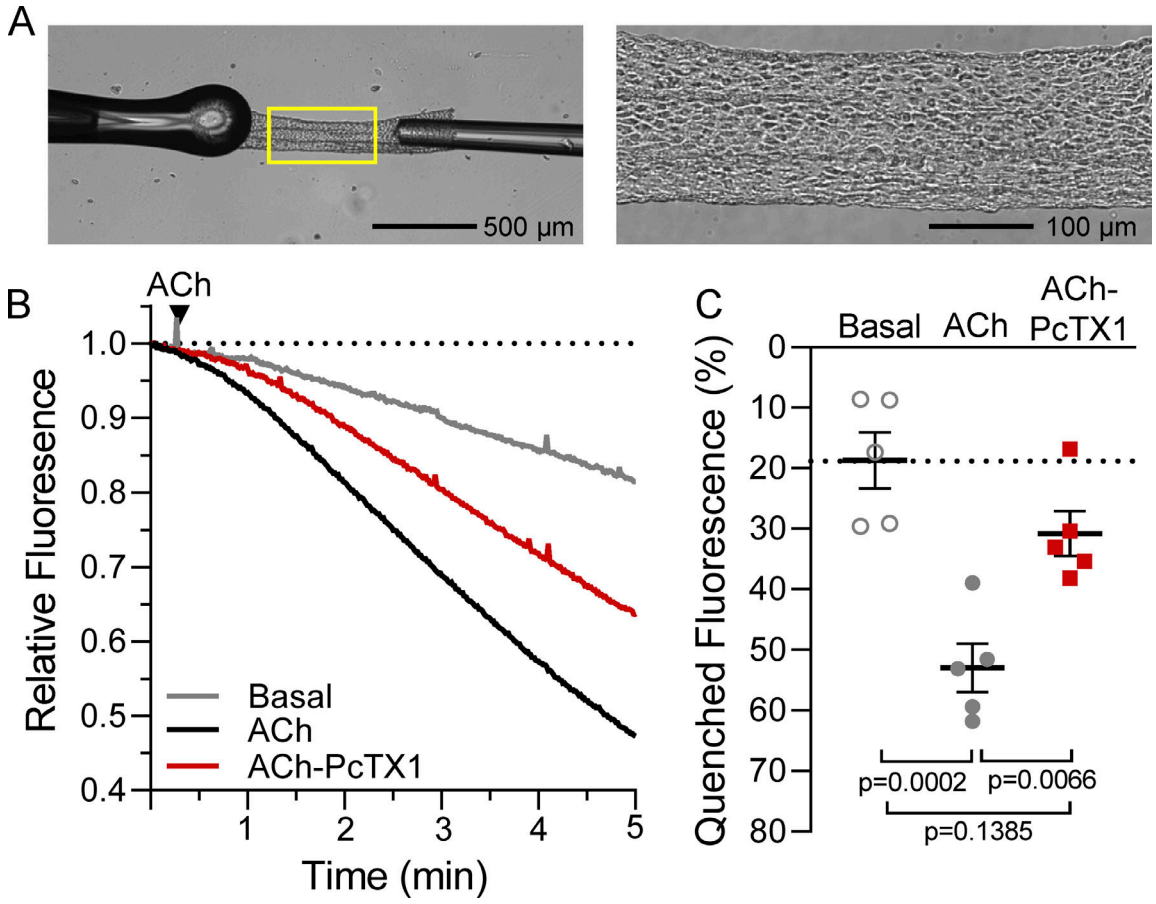

Figure 4. **ASIC1a contributes to ACh-induced Ca^{2+} entry in mesenteric endothelial tubes. (A)** Endothelial tubes were freshly isolated and loaded with fura-2. **(B)** Averaged traces showing Mn^{2+}-quenching of fura-2 fluorescence at 360 nm excitation. Experiments were conducted under basal conditions or following ACh (10^{-6} M) in the absence or presence of PcTX1 (20 nM). **(C)** Summary data for percent quenched fura-2 fluorescence by Mn^{2+} at 5 min. Dotted line represents mean basal values. Data represent biological replicates and were analyzed by two-way ANOVA. The two-way ANOVA revealed that there was a statistically significant interaction (P = 0.0003) between factors. Post-hoc pairwise comparisons were analyzed between individual groups using Tukey's multiple comparisons test.

P = 0.3450). Together these data support a potential interaction between ASIC1 and both IK_{Ca} and SK_{Ca} channels. Fig. 6 E shows autofluorescence of the IEL and immunofluorescence of ASIC1 localized within fenestrations of the IEL, which represent areas of myoendothelial junctions and EDH signaling.

ASIC1 activates IK_{Ca}/SK_{Ca} channels

Mesenteric endothelial cells were positively identified by staining with tomato lectin (Fig. 7 A) and had a mean capacitance of 10.4 ± 0.5 pF (n = 49). The recorded K^+ currents in endothelial cells were relatively small and mostly fast-activating and non-inactivating, as shown in Fig. 7 B. Consistent with other reports (Ledoux et al., 2008), the whole-cell currents recorded from voltage steps exhibited inward rectification at positive membrane potentials. Treatment with Tram-34/Apamin, but not PcTX1, significantly reduced baseline K^+ currents at −140 to −120 and 20 to 80 mV (Fig. 7, C and E–F; and Table 3), suggesting the presence of basal IK_{Ca}/SK_{Ca} activity. ACh caused a substantial increase in endothelial IK_{Ca}/SK_{Ca}-dependent currents at all voltages except −60 mV (Fig. 7, D–F and Table 3). These ACh-induced IK_{Ca}/SK_{Ca} currents were prevented by treatment with Tram-34/Apamin or PcTX1 (Fig. 7, D and E–F and Table 3). Fig. 7 G shows that the majority of both the basal and ACh-induced K^+ currents are sensitive to both Tram-34/Apamin or PcTX1, suggesting an essential role for ASIC1 in the ACh-mediated activation of IK_{Ca}/SK_{Ca} channels in mesenteric endothelial cells.

To determine if direct stimulation of ASIC1 leads to vasodilation and activation of IK_{Ca}/SK_{Ca} channels, we used the selective agonist, α/β-MitTx. Since α/β-MitTx is a large, membrane-impermeable peptide, we luminally perfused preconstricted isolated mesenteric arteries with α/β-MitTx (Fig. 8 A). PcTX1 largely diminished α/β-MitTx demonstrating ASIC1-mediated vasodilation (Fig. 8 B). α/β-MitTx vasodilatory responses were unaffected by L-NNA and indomethacin, suggesting that the activation of ASIC1 does not stimulate endothelial NO synthase (eNOS) or cyclooxygenases (Fig. 8, A and B). Inhibition of IK_{Ca}/SK_{Ca} largely attenuated the α/β-MitTx vasodilatory response (Fig. 8, A and B). Furthermore, α/β-MitTx significantly increased K^+ currents that were subsequently blocked by treatment with either Tram-34/Apamin or PcTX1 (Fig. 8, C–F and

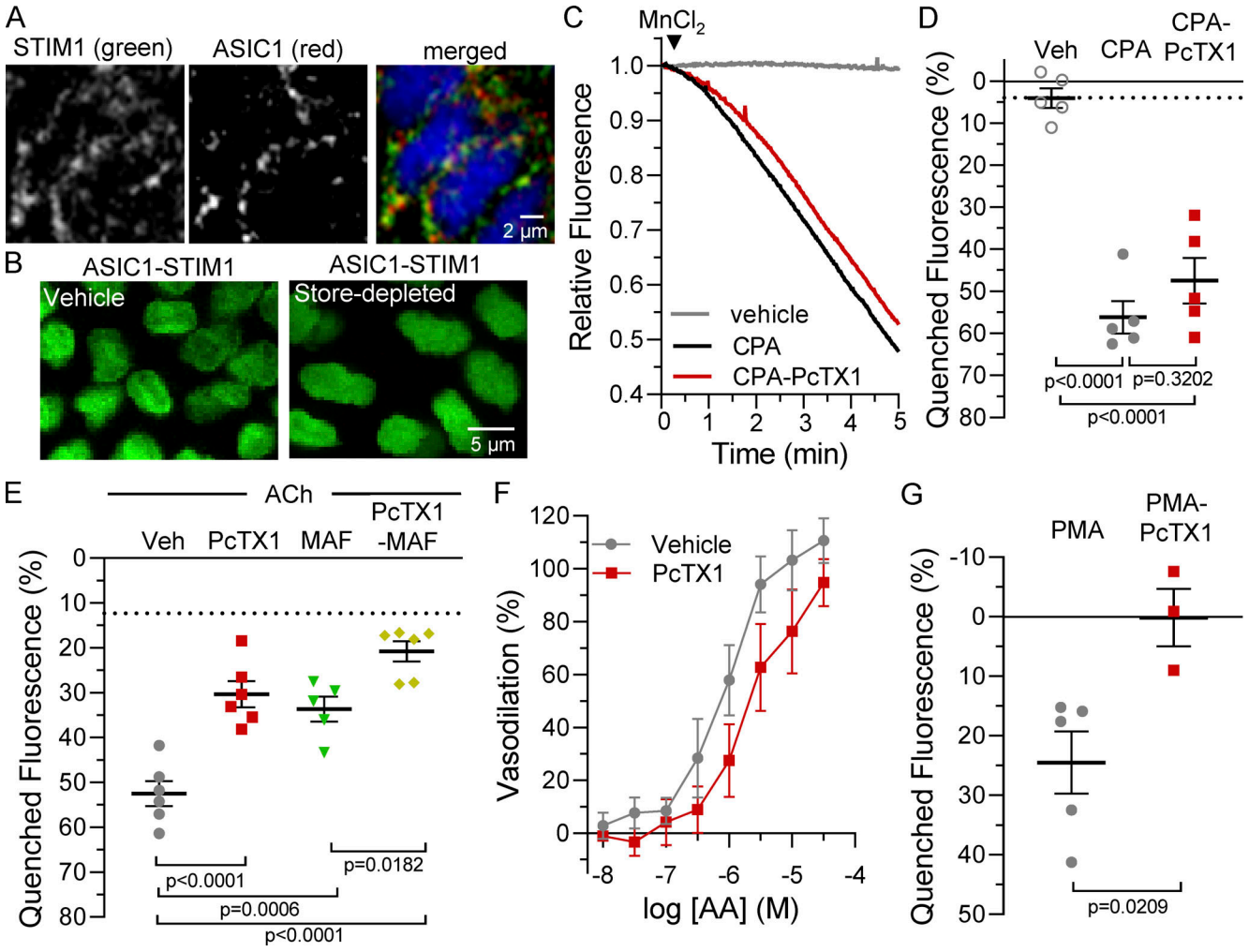

Figure 5. **PKC activates ASIC1 in mesenteric endothelial tubes. (A)** Representative immunofluorescence images in mesenteric endothelial tubes showing ASIC1a (red) and STIM-1 (green) distribution. Nuclei are stained with Sytox (blue). **(B)** Representative images showing lack of Duolink proximity ligation interaction between ASIC1–STIM1 (no observed red puncta). **(C and D)** Averaged traces (C) and summary data (D) showing Mn^{2+}-quenching of fura-2 fluorescence (%) at 360 nm excitation. $MnCl_2$ (500 µM) was added under vehicle conditions (0 Ca^{2+}) or in the absence or presence of PcTX1 (20 nM) following incubation with CPA (10 µM) to deplete intracellular Ca^{2+} stores. Dotted line represents the absence of CPA (Veh). **(E)** Summary data showing Mn^{2+}-quenching of fura-2 fluorescence (%) under basal conditions (dotted line) or following 5 min ACh (10^{-6} M) in the absence or presence of PLA_2 inhibitor, MAF (5 µM), and/or PcTX1 (20 nM). Data in D and E represent biological replicates and were analyzed by one-way ANOVA. Post-hoc pairwise comparisons were analyzed between individual groups using Tukey's multiple comparisons test. **(F)** Vasodilation responses to AA (10^{-8} to 3×10^{-5} M) following preconstriction with U-46619 in mesenteric arteries. **(G)** Summary data showing Mn^{2+}-quenching of fura-2 fluorescence (%) following 10 min PMA (10^{-5} M) in the absence or presence of PcTX1 (20 nM). Biological replicates were analyzed by unpaired *t* tests.

Table 3), suggesting activation of ASIC1 stimulates IK_{Ca}/SK_{Ca} currents.

Discussion

Studies directly assessing the role of ASIC1a in the vasculature are limited and mainly focus on the expression of ASIC1a in smooth muscle. The current study aims to examine the unique role of ASIC1a in the endothelium of small mesenteric resistance arteries. We found inhibition of ASIC1a largely blunted the sustained vasodilatory response and endothelial Ca^{2+} influx in response to ACh. Further investigation found that activation of ASIC1a leads to stimulation of IK_{Ca} and SK_{Ca} to mediate EDH-dependent vasodilation (Fig. 9). Collectively, these data provide novel evidence that ASIC1a is a functional ion channel in rat mesenteric endothelial cells and a fundamental component of the EDH pathway.

ASICs were first recognized in cardiovascular homeostasis as important signaling molecules in sensory neurons. ASIC2 has been shown to function as the mechanosensing molecule in baroreceptors (Lu et al., 2009), and ASIC3 has been implicated in the transduction of acid sensitivity by peripheral and central chemoreceptors (Tan et al., 2010; Lu et al., 2013; Song et al., 2016; Huda et al., 2012). ASIC1a can also regulate vascular function through neural sensory signaling; however, the specific role of ASIC1a varies widely among different vascular beds. ASIC1a expressed in cardiac muscle afferents contributes to myocardial ischemic-reperfusion injury (Redd et al., 2021). In

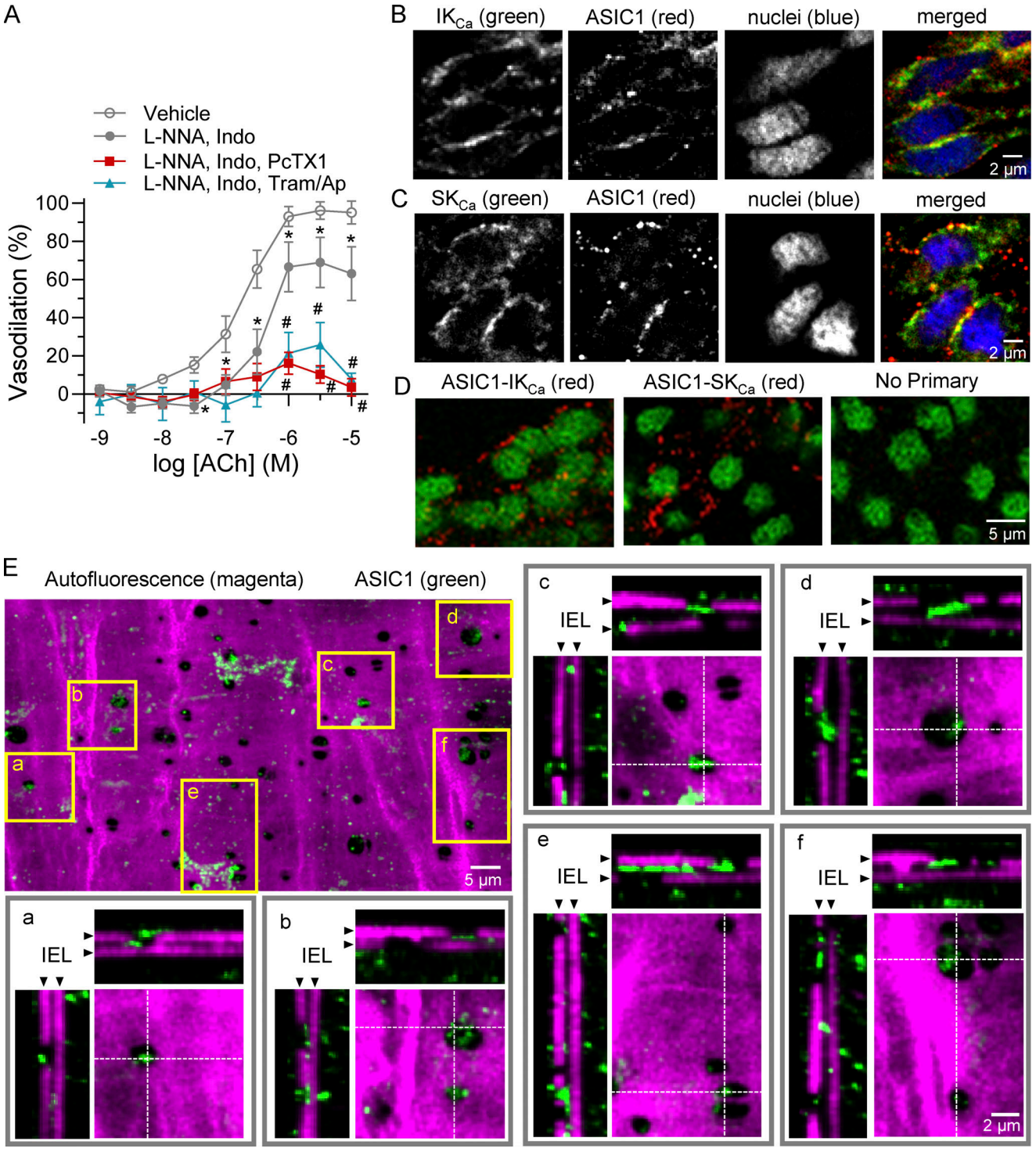

Figure 6. **ASIC1 contributes to endothelium-dependent, hyperpolarization-induced vasodilation, colocalizes with IK_{Ca} and SK_{Ca} channels, and localizes within myoendothelial junctions. (A)** ACh (10^{-9}–10^{-5} M) induced vasodilatory responses in mesenteric arteries, in the absence or presence of the NOS-specific inhibitor L-NNA (100 µM), the cyclooxygenase specific inhibitor indomethacin (Indo; 10 µM), and either PcTX1 (20 nM) or Tram-34 and Apamin (Tram/Ap; 1 µM and 100 nM, respectively). Data represent five animals (biological replicates)/group and were analyzed by two-way ANOVA. The two-way ANOVA revealed that there was a statistically significant interaction ($P < 0.0001$) between factors. Post hoc pairwise comparisons were analyzed between individual groups using Tukey's multiple comparisons test. *$P < 0.05$ vehicle vs. L-NNA, Indo; #$P < 0.05$ L-NNA, Indo alone vs. PcTX1 or Tram/Ap. P values for data in A are shown in Table 2. **(B and C)** Immunofluorescence in mesenteric endothelial tubes showing ASIC1a (red) and (B) IK_{Ca} (green) or (C) SK_{Ca} (green) distribution. Nuclei are stained with Sytox (blue). **(D)** Representative images showing the Duolink proximity ligation interaction between ASIC1-IK_{Ca}, ASIC1-SK_{Ca}, or no primary antibodies as a negative control. **(E)** Autofluorescence (magenta) of the IEL and immunofluorescence of ASIC1 (green) in an intact, whole-mount mesenteric artery. Areas without magenta demonstrate fenestrations in IEL associated with myoendothelial junctions. Magnified images (a-f; yellow boxes) show the orthogonal view of the IEL layers (arrows), with the smooth muscle on the outside and endothelium between the IEL layers.

Table 2. **P values for data in Fig. 6**

Log [ACh] (M):	**−9**	**−8.5**	**−8**	**−7.5**	**−7**	**−6.5**	**−6**	**−5.5**	**−5**
Veh vs. L-NNA, Indo	0.6386	0.1156	0.091	**0.0012**	**0.0169**	**0.0097**	**0.0441**	**0.0426**	**0.0432**
All in the presence of L-NNA, Indo									
Veh vs. PcTX1	0.9697	0.3630	0.9712	0.4479	0.9744	0.6251	**0.0184**	**0.0086**	**0.0116**
Veh vs. Tram/AP	0.7449	0.5454	0.9996	0.5537	0.5960	0.3092	**0.0426**	**0.0437**	**0.0169**
PcTX1 vs. Tram/AP	0.7875	0.9744	0.9909	0.9752	0.5357	0.6873	0.9069	0.4692	0.7627
Repeated-measures, BL vs. 10^{-9} to 10^{-5} [ACh] (indicates [ACh] affect on diameter)									
Vehicle	0.8836	0.8285	0.4802	**0.0145**	**<0.0001**	**<0.0001**	**<0.0001**	**<0.0001**	**<0.0001**
L-NNA, Indo	0.2808	0.6559	0.6334	0.9374	0.5581	**0.0130**	**0.0122**	**0.0232**	**0.0285**
L-NNA, Indo, PcTX1	0.4846	0.3019	0.9983	0.9022	0.7495	0.2803	0.5386	0.9878	0.8413
L-NNA, Indo, Tram/AP	0.9370	0.9979	0.9880	0.9998	0.9932	0.1773	0.1307	0.3101	0.3972

Data represent biological replicates and were analyzed by two-way ANOVA. The two-way ANOVA revealed that there was a statistically significant interaction ($P < 0.0001$) between factors. Post hoc pairwise comparisons were analyzed between individual groups using Tukey's multiple comparisons test. $P < 0.05$ (bold text) is considered significantly different.

skeletal muscle afferents, ASIC1a participates in the exercise pressor reflex (Ducrocq et al., 2020), consistent with findings that ASIC1a opposes functional hyperemia and exercise capacity in the skeletal muscle circulation (Drummond et al., 2017). However, this effect of ASIC1a was not mediated by reducing the ability of vessels to dilate, but rather ASIC1a appears to limit vascular recruitment in the hind limb skeletal muscle bed (Drummond et al., 2017). Although ASICs can regulate the cardiovascular system through neural sensory signaling, the more recent identification of non-neuronal expression of ASICs in vascular tissue indicates a possible involvement of ASICs to modulate vascular tone intrinsically.

The functional role of ASIC1 in the vasculature may be further complicated by the differential expression of ASIC1 in vascular smooth muscle and endothelial cells. In small pulmonary arteries, ASIC1a is more abundantly expressed in smooth muscle cells than endothelial cells. Pulmonary arterial smooth muscle cell Ca^{2+} influx contributes to agonist- and hypoxia-induced vasoconstriction (Nitta et al., 2014). Our previous findings also demonstrate a pathological function of smooth muscle ASIC1a in developing pulmonary hypertension by contributing to the persistent pulmonary arterial smooth muscle cell membrane depolarization, hyperreactivity, and vascular remodeling (Nitta et al., 2014; Jernigan et al., 2021; Garcia et al., 2022). ASIC1 has also been detected in cerebral artery smooth muscle cells (Chung et al., 2011; Lin et al., 2014), where the H^+-induced ASIC-like currents appear to be predominantly formed by ASIC1b (Chung et al., 2011). However, whether this cerebral smooth muscle ASIC1 contributes to vasoconstriction has not been assessed. Despite the expression of ASIC1 in smooth muscle cells of mesenteric resistance arteries, we have not been able to demonstrate a functional role for ASIC1 in mediating PE- or endothelin-1–induced vasoconstriction (Garcia et al., 2020). Rather, the augmentation of endothelin-1–induced vasoconstriction at lower concentrations prompted us to investigate the potential role of ASIC1a in mediating vasodilation via expression in the endothelium.

Although ASIC1 is classically known to be activated by extracellular acidosis and H^+, several non-proton mechanisms have also been described, including activation following stimulation of G-protein coupled receptors (GPCRs; Fig. 9). However, the molecular mechanism through which ACh activates ASIC1a in endothelial cells is not known. Cleavage of phosphatidylinositol 4,5-bisphosphate ($PI(4,5)P_2$) by GqPCR-activated phospholipase C (PLC) generates two second messengers: membrane-bound lipid diacylglycerol (DAG) and soluble inositol 1,4,5-trisphosphate (IP_3). Depleting $PI(4,5)P_2$ during PLC signaling has inhibitory or potentiating effects on the activity of several ion channels, including members of the transient receptor potential (TRP) channel family (Suh and Hille, 2008). However, previous studies indicate ASIC1 activity is independent of membrane phosphoinositides such as PI(4)P, $PI(4,5)P_2$, and possibly $PI(3,4,5)P_3$ (Kweon et al., 2015). We have previously shown that ASIC1a is activated secondary to sarcoplasmic reticulum Ca^{2+} store depletion (IP_3-mediated mechanism) in pulmonary arterial smooth muscle cells (Jernigan et al., 2009; Garcia et al., 2020). Although there is a robust SOCE response, this mechanism does not activate ASIC1a in mesenteric endothelial cells, suggesting that ASIC1a-dependent calcium influx is mediated through a receptor-operated pathway. AA and lysophosphocholine have also been identified as endogenous non-proton ligands that can activate ASICs in a neutral pH environment (Marra et al., 2016; Smith et al., 2007). Although the PLA_2–AA pathway was activated following ACh, ASIC1a was not activated by AA. Additionally, several studies, including one from our laboratory, show that ASIC1a channel function is directly regulated by PKC (Ren et al., 2016; Qiu et al., 2012; Herbert et al., 2016; Hu et al., 2010; Zhang et al., 2020; Berdiev et al., 2002; Li et al., 2019; Baron et al., 2002). Although we did not determine the specific PKC isoforms activated in response to ACh in mesenteric endothelial cells, Adapala and colleagues found that PKCα mediates ACh-induced transient receptor potential vanilloid 4 (TRPV4)-dependent calcium influx in mouse dermal vascular endothelial cells (Adapala et al., 2011). These data indicate PKC signaling is activated by ACh in endothelial cells; however,

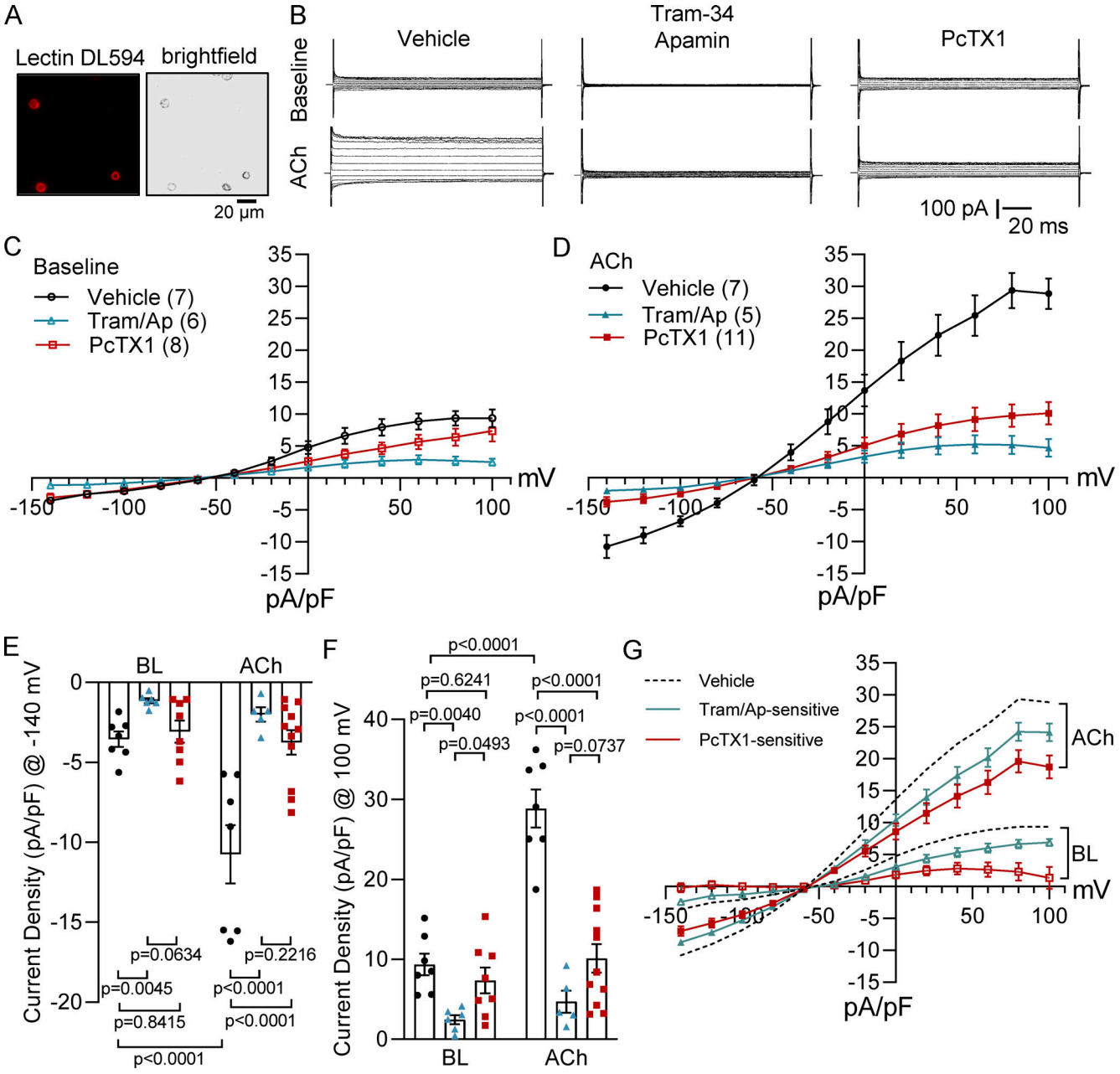

Figure 7. **ASIC1 inhibition abolishes ACh-induced IK_{Ca}/SK_{Ca} currents. (A)** Representative fluorescence and brightfield images showing identification of lectin-stain endothelial cells. **(B–D)** Representative K^+ current traces and average current density (pA/pF) plotted as a function of voltage (mV) recorded in freshly dispersed mesenteric endothelial cells during baseline conditions (C) and following 1 µM ACh (D) in the presence of vehicle (black circles), PcTX1 (20 nM, red triangles), or Tram-34 (1 µM) and Apamin (100 nM; blue squares). Data represent biological replicates (noted in parentheses) and were analyzed by two-way ANOVA. The two-way ANOVA revealed that there was a statistically significant interaction ($P < 0.0001$) between factors. **(E and F)** Post-hoc pairwise comparisons were analyzed between individual groups using Tukey's multiple comparisons test and the P values are given in Table 3 and summary data for −140 mV (E) and 100 mV (F). **(G)** Summary data showing Tram/Ap-sensitive and PcTX1-sensitive K^+ currents under baseline conditions or following ACh.

future investigation is needed to determine the specific PKC isoform regulating ASIC1 in the endothelium. Although other secondary mechanisms may result in the activation of ASIC1a following GPCR stimulation, the current data suggest that ASIC1a may be activated by ACh via PLC–DAG–PKC signaling.

ASIC1a has been shown to contribute to hypercapnia-induced NO production and vasodilation in cerebral arteries (Faraci et al., 2019). However, this has been attributed to neuronal ASIC1a since neuronal-specific ASIC1a knockout mice similarly showed decreased hypercapnia-induced vasodilation. In addition, ACh-induced cerebral vasodilation was intact following PcTX1 or global knockout of ASIC1a, suggesting the effects of ASIC1a were independent of the endothelium or eNOS (Faraci et al., 2019). This difference in the involvement of ASIC1a to ACh-induced vasodilation observed between cerebral and mesenteric arteries is likely a result of the heterogeneous expression

Table 3. **P values for data in Figs. 7, and 8**

VOLTAGE (mV):	−120	−100	−80	−60	−40	−20	0	20	40	60	80
BL vs. ACh											
Vehicle	**<0.0001**	**<0.0001**	**0.0001**	0.9360	**0.0036**	**0.0004**	**0.0002**	**<0.0001**	**<0.0001**	**<0.0001**	**<0.0001**
Tram/AP	0.9018	0.8199	0.9510	0.9995	0.9131	0.8718	0.8502	0.8353	0.8317	0.8245	0.7961
PcTX1	0.8247	0.8242	0.9230	0.9596	0.6034	0.4723	0.4186	0.3843	0.3591	0.3803	0.3697
BL: Veh vs.											
Tram/AP	**0.0478**	0.0565	0.1170	0.9360	0.7679	0.1394	0.0582	**0.0309**	**0.0146**	**0.0054**	**0.0017**
PcTX1	0.9996	0.9431	0.8851	0.9995	0.8938	0.363	0.2181	0.173	0.1455	0.1734	0.2547
ACh: Veh vs.											
Tram/AP	**<0.0001**	**<0.0001**	**<0.0001**	0.8409	**0.0168**	**0.0006**	**<0.0001**	**<0.0001**	**<0.0001**	**<0.0001**	**<0.0001**
PcTX1	**<0.0001**	**<0.0001**	**<0.0001**	0.8680	**0.0119**	**0.0004**	**<0.0001**	**<0.0001**	**<0.0001**	**<0.0001**	**<0.0001**
BL vs. MitTx	**0.0004**	**0.0021**	**0.0111**	0.8656	0.1122	0.1051	0.1349	0.1016	0.0635	**0.0476**	**0.0348**
MitTx: Veh vs.											
Tram/AP	**0.0020**	**0.0025**	**0.0030**	0.1121	0.0742	**0.0394**	**0.0283**	**0.0230**	**0.0200**	**0.0247**	**0.0216**
PcTX1	**0.0055**	**0.0098**	**0.0130**	0.3158	0.1998	0.1108	0.0791	0.0579	**0.0440**	**0.0465**	**0.0380**

Data represent biological replicates and were analyzed by two-way ANOVA. The two-way ANOVA revealed that there was a statistically significant interaction ($P < 0.0001$) between factors. Post-hoc pairwise comparisons were analyzed between individual groups using Tukey's multiple comparisons test. $P < 0.05$ (bold text) is considered significantly different.

of ASIC1a in the endothelium and/or the predominant signaling pathway (NO, PGI_2, or EDH) evoked by the increase in endothelial intracellular Ca^{2+} following ACh stimulation.

The contribution of EDH to endothelium-dependent vasodilation is inversely related to vessel size, where large conduit arteries rely mostly on NO, and small resistance arteries are more likely to rely on EDH to mediate vasodilation (Nagao et al., 1992; Clark and Fuchs, 1997; Zhang et al., 2007). However, EDH contributes very little to vasodilation in some vascular beds, regardless of artery size. In the cerebral arteries, Farcai et al. (2019) demonstrated that ACh-induced vasodilation was predominately mediated by NO; whereas, in mesenteric arteries, we show >60% of the ACh-induced vasodilation is independent of NO or cyclooxygenase products. This remaining vasodilation in mesenteric arteries was abolished by either IK_{Ca}/SK_{Ca} or ASIC1a inhibition, suggesting a common pathway.

While we did not directly assess ASIC1-induced subcellular Ca^{2+} events, ASIC1 signaling is likely dependent on the microdomain in which the channel resides. Indeed, this has been recently shown for TRPV4 channels, where TRPV4 preferentially couple with IK_{Ca}/SK_{Ca} channels in mesenteric endothelial cells and with eNOS in pulmonary endothelial cells (Ottolini et al., 2020). Like TRPV4, ASIC1a may regulate the activation of IK_{Ca} and SK_{Ca} channels by locally increasing the Ca^{2+} concentration near IK_{Ca}/SK_{Ca} to activate these channels (Sonkusare et al., 2012). We observed Na^+/Ca^{2+} permeability ratios of ∼2.0 in freshly isolated pulmonary arterial smooth muscle cells and 2.5 in acutely cultured pulmonary arterial smooth muscle cells (Jernigan et al., 2009), which are consistent with the reported ASIC1a Na^+/Ca^{2+} permeability ratios of 2.5 in *Xenopus* oocytes (Waldmann et al., 1997b). Both IK_{Ca} and SK_{Ca} are voltage-independent and highly sensitive to a rise in intracellular $[Ca^{2+}]$ with activation in the 200–500 nM range (Ishii et al., 1997; Xia et al., 1998; Köhler et al., 1996). A local influx of Ca^{2+} through ASIC1 would be sufficient to activate IK_{Ca}/SK_{Ca}. An additional possibility is a physical protein–protein interaction between ASIC1 and IK_{Ca}/SK_{Ca}. Previous studies have shown that under basal conditions, ASIC1a interacts with big-conductance Ca^{2+}-activated K^+ (BK_{Ca}) channels and inhibits their current in both HEK293 cells and neurons (Petroff et al., 2008, 2012; Wang et al., 2015). Activation of ASIC1a disrupts this inhibitory association with BK_{Ca}, leading to increased BK_{Ca} channel activity (Petroff et al., 2008; Petroff et al., 2012; Wang et al., 2015). These studies did not examine the possibility that activation of ASIC1a, and subsequent Na^+-dependent depolarization and/or Ca^{2+} influx, elicits BK_{Ca} channel activity. Rather, Petroff et al. (2008) indicate that the effect of ASIC1a to inhibit BK_{Ca} results from a direct inhibitory interaction of extracellular domains as mutations in ASIC1a or ASIC gene disruption (*Asic1/2/3* triple knockout) results in augmented K^+ channel currents in cortical neurons (Petroff et al., 2012). Although we do not know if there is a similar direct interaction between ASIC1 and IK_{Ca} or SK_{Ca}, our data demonstrate that ASIC1 colocalizes with IK_{Ca}/SK_{Ca} channels, and direct stimulation of ASIC1 with α/β-MitTx activates IK_{Ca}/SK_{Ca} currents in mesenteric endothelial cells and dilates mesenteric arteries.

Although significant progress has been made in understanding the importance of ASIC1a in regulating vascular tone, many questions remain unanswered. ASIC1a is uniquely permeable to Ca^{2+} compared with other ASIC channels (Xiong et al.,

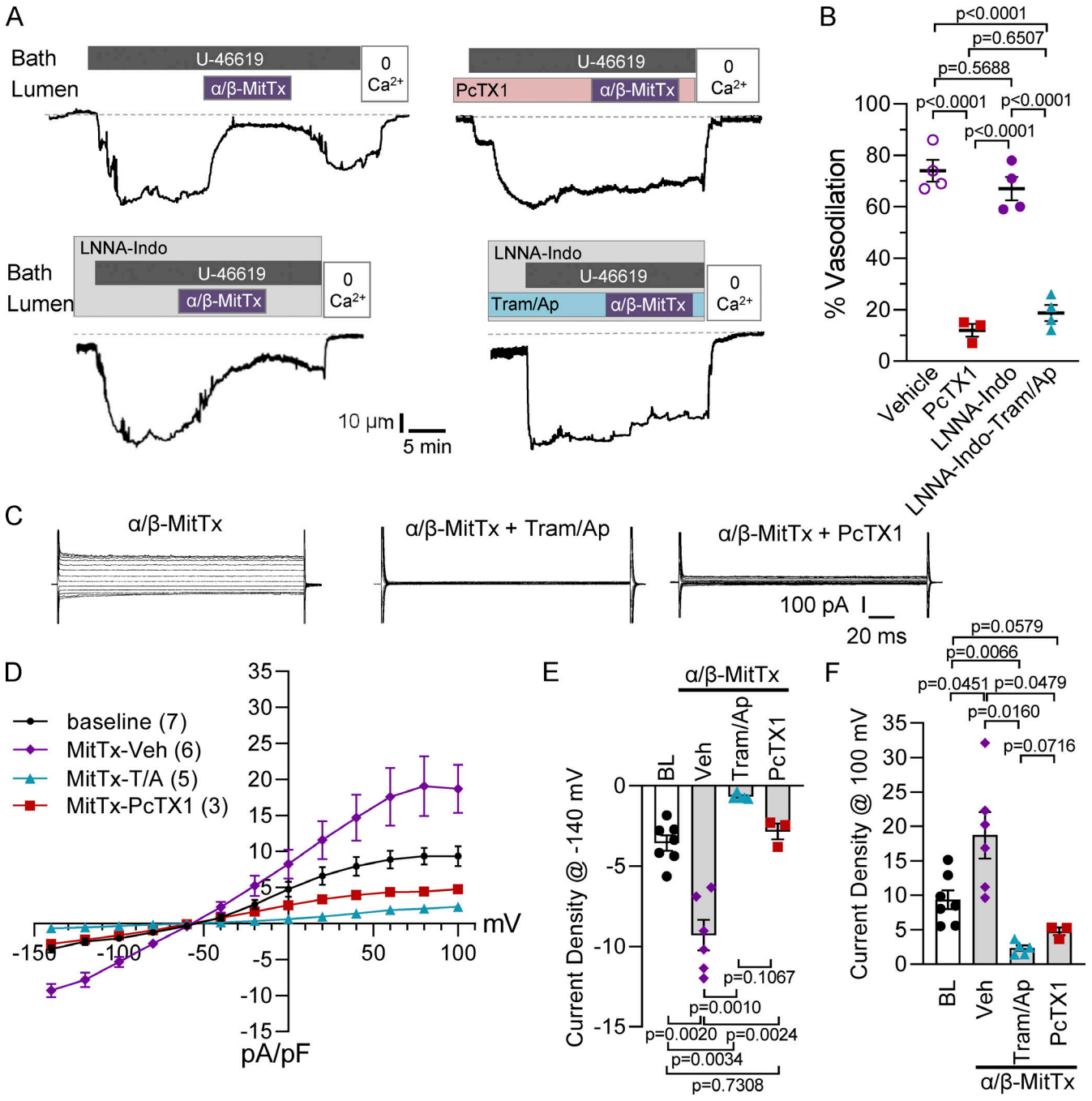

Figure 8. **Direct stimulation of ASIC1 causes vasodilation and activates IK_{Ca}/SK_{Ca} currents. (A and B)** Representative trace showing changes in vessel inner diameter (µm; A) and summary data showing percent vasodilation in response to luminal perfusion of α/β-MitTx (200 nM bolus; B) in preconstricted mesenteric arteries in the presence of vehicle, PcTX1, LNNA-Indo, or LNNA-Indo-TRAM/Ap. Data represent biological replicates and were analyzed by one-way ANOVA. Post-hoc pairwise comparisons were analyzed between individual groups using Tukey's multiple comparisons test. **(C and D)** Representative K^+ current traces (C) and average current density (pA/pF; D) plotted as a function of voltage (mV) recorded in freshly dispersed mesenteric endothelial cells during baseline (from Fig. 7 B) and following activation of ASIC1 with α/β-MitTx (20 nM; purple diamond) in the absence or presence of PcTX1 (20 nM, red squares) or Tram-34 (1 µM) and Apamin (100 nM; blue triangles). Data represent biological replicates (noted in parentheses) and were analyzed by two-way ANOVA. The two-way ANOVA revealed that there was a statistically significant interaction ($P < 0.0001$) between factors. **(E and F)** Post-hoc pairwise comparisons were analyzed between individual groups using Tukey's multiple comparisons test and the P values are given in Table 3 and in summary data for −140 mV (E) and 100 mV (F).

2004; Yermolaieva et al., 2004), which leads to distinct intracellular signaling events within both vascular smooth muscle and endothelial cells. Therefore, it is essential to further investigate the role of ASIC1 in other vascular beds. The possibility that ASIC1 contributes to the intrinsic regulation of blood flow makes them a prime therapeutic target for cardiovascular disease, considering they are activated under acidosis, ischemia, and inflammatory conditions. Furthermore, our research

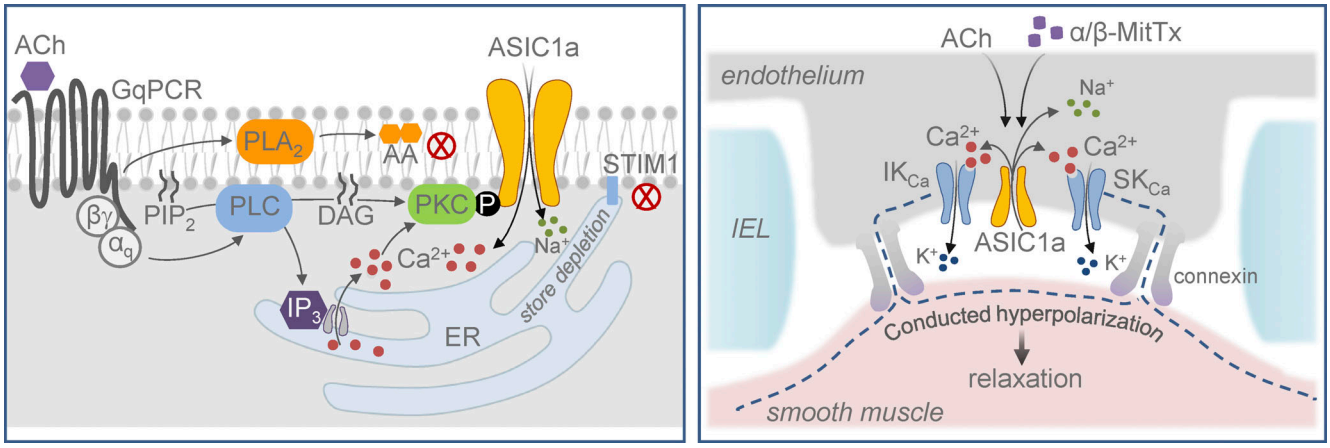

Figure 9. **ASIC1a signaling in mesenteric endothelial cells.** Left: In mesenteric endothelial cells, ASIC1a is activated by ACh. In the present study, we show this is likely due to the secondary activation via PKC, and not through endoplasmic reticulum (ER) store-depletion mechanisms involving STIM1 or AA. Right: Myoendothelial junction showing the presence of ASIC1a in the fenestrations of the IEL where it contributes to ACh-induced endothelium-dependent dilation through activation of IK_{Ca}/SK_{Ca} channels.

suggests ASIC1a can be activated by a variety of stimuli independent of H^+. Defining the molecular mechanism(s) involved in the regulation of ASIC1a function will not only advance our understanding of the pathogenesis of cardiovascular disease but will also help identify a novel target(s) for therapeutic intervention.

Acknowledgments

Jeanne M. Nerbonne served as editor.

The authors thank Lindsay Herbert for her research technical support, Tamara Howard for help in processing tissue for immunofluorescence experiments, and Dr. Michael Paffett (UNM Comprehensive Cancer Center [CCC]) for technical assistance with immunofluorescence imaging.

This work was supported by the National Heart, Lung and Blood Institute grants R01 HL111084 (to N.L. Jernigan), R01 HL160606 (to J.S. Naik), F31 HL145836 (to S.M. Garcia), and T32 HL007736 (to T.C. Resta). This research made use of the Fluorescence Microscopy and Cell Imaging Shared Resource, which is supported by UNM CCC Support Grant NCI P30CA118100.

The authors declare no competing financial interests.

Author Contributions: All persons designated as authors qualify for authorship, and all those who qualify for authorship are listed. S.M. Garcia and N.L. Jernigan contributed to the concept, design, acquisition, analysis, interpretation, and drafting/revising of the work. J.S. Naik and T.C. Resta contributed to the concept, design, interpretation, and revising of the work for important intellectual content. All authors approved the final version of the manuscript and agree to be accountable for all aspects of the work in ensuring that questions related to the accuracy or integrity of any part of the work are appropriately investigated and resolved.

Submitted: 12 April 2022
Revised: 21 October 2022
Accepted: 17 November 2022

References

Adapala, R.K., P.K. Talasila, I.N. Bratz, D.X. Zhang, M. Suzuki, J.G. Meszaros, and C.K. Thodeti. 2011. PKCα mediates acetylcholine-induced activation of TRPV4-dependent calcium influx in endothelial cells. *Am. J. Physiol. Heart Circ. Physiol.* 301:H757–H765. https://doi.org/10.1152/ajpheart.00142.2011

Akanji, O., N. Weinzierl, R. Schubert, and L. Schilling. 2019. Acid sensing ion channels in rat cerebral arteries: Probing the expression pattern and vasomotor activity. *Life Sci.* 227:193–200. https://doi.org/10.1016/j.lfs.2019.04.054

Baron, A., E. Deval, M. Salinas, E. Lingueglia, N. Voilley, and M. Lazdunski. 2002. Protein kinase C stimulates the acid-sensing ion channel ASIC2a via the PDZ domain-containing protein PICK1. *J. Biol. Chem.* 277: 50463–50468. https://doi.org/10.1074/jbc.M208848200

Bashari, E., Y.J. Qadri, Z.-H. Zhou, N. Kapoor, S.J. Anderson, R.H. Meltzer, C.M. Fuller, and D.J. Benos. 2009. Two PKC consensus sites on human acid-sensing ion channel 1b differentially regulate its function. *Am. J. Physiol. Cell Physiol.* 296:C372–C384. https://doi.org/10.1152/ajpcell.00200.2008

Benarroch, E.E. 2014. Acid-sensing cation channels: Structure, function, and pathophysiologic implications. *Neurology*. 82:628–635. https://doi.org/10.1212/WNL.0000000000000134

Berdiev, B.K., J. Xia, B. Jovov, J.M. Markert, T.B. Mapstone, G.Y. Gillespie, C.M. Fuller, J.K. Bubien, and D.J. Benos. 2002. Protein kinase C isoform antagonism controls BNaC2 (ASIC1) function. *J. Biol. Chem.* 277: 45734–45740. https://doi.org/10.1074/jbc.M208995200

Brandes, R.P., F.H. Schmitz-Winnenthal, M. Félétou, A. Gödecke, P.L. Huang, P.M. Vanhoutte, I. Fleming, and R. Busse. 2000. An endothelium-derived hyperpolarizing factor distinct from NO and prostacyclin is a major endothelium-dependent vasodilator in resistance vessels of wild-type and endothelial NO synthase knockout mice. *Proc. Natl. Acad. Sci. USA*. 97:9747–9752. https://doi.org/10.1073/pnas.97.17.9747

Chen, C.-C., S. England, A.N. Akopian, and J.N. Wood. 1998. A sensory neuron-specific, proton-gated ion channel. *Proc. Natl. Acad. Sci. USA*. 95: 10240–10245. https://doi.org/10.1073/pnas.95.17.10240

Chung, W.S., J.M. Farley, and H.A. Drummond. 2011. ASIC-like currents in freshly isolated cerebral artery smooth muscle cells are inhibited by endogenous oxidase activity. *Cell. Physiol. Biochem.* 27:129–138. https://doi.org/10.1159/000325215

Clark, S.G., and L.C. Fuchs. 1997. Role of nitric oxide and Ca^{++}-dependent K^+ channels in mediating heterogeneous microvascular responses to acetylcholine in different vascular beds. *J. Pharmacol. Exp. Ther.* 282:1473–1479

Clozel, M., G.A. Gray, V. Breu, B.M. Löffler, and R. Osterwalder. 1992. The endothelin ETB receptor mediates both vasodilation and vasoconstriction in vivo. *Biochem. Biophys. Res. Commun.* 186:867–873. https://doi.org/10.1016/0006-291x(92)90826-7

Czikora, I., A.A. Alli, S. Sridhar, M.A. Matthay, H. Pillich, M. Hudel, B. Berisha, B. Gorshkov, M.J. Romero, J. Gonzales, et al. 2017. Epithelial

sodium channel-α mediates the protective effect of the TNF-derived TIP peptide in pneumolysin-induced endothelial barrier dysfunction. *Front. Immunol.* 8:842. https://doi.org/10.3389/fimmu.2017.00842

Drummond, H.A., L. Xiang, A.R. Chade, and R. Hester. 2017. Enhanced maximal exercise capacity, vasodilation to electrical muscle contraction, and hind limb vascular density in ASIC1a null mice. *Physiol. Rep.* 5: e13368. https://doi.org/10.14814/phy2.13368

Ducrocq, G.P., J.S. Kim, J.A. Estrada, and M.P. Kaufman. 2020. ASIC1a plays a key role in evoking the metabolic component of the exercise pressor reflex in rats. *Am. J. Physiol. Heart Circ. Physiol.* 318:H78–H89. https://doi.org/10.1152/ajpheart.00565.2019

Faraci, F.M., R.J. Taugher, C. Lynch, R. Fan, S. Gupta, and J.A. Wemmie. 2019. Acid-sensing ion channels: Novel mediators of cerebral vascular responses. *Circ. Res.* 125:907–920. https://doi.org/10.1161/CIRCRESAHA.119.315024

Garcia, S.M., L.M. Herbert, B.R. Walker, T.C. Resta, and N.L. Jernigan. 2020. Coupling of store-operated calcium entry to vasoconstriction is acid-sensing ion channel 1a dependent in pulmonary but not mesenteric arteries. *PLoS One.* 15:e0236288. https://doi.org/10.1371/journal.pone.0236288

Garcia, S.M., T.R. Yellowhair, N.D. Detweiler, R. Ahmadian, L.M. Herbert, L.V. Gonzalez Bosc, T.C. Resta, and N.L. Jernigan. 2022. Smooth muscle acid-sensing ion channel 1a as a therapeutic target to reverse hypoxic pulmonary hypertension. *Front. Mol. Biosci.* 9:989809. https://doi.org/10.3389/fmolb.2022.989809

García-Añoveros, J., B. Derfler, J. Neville-Golden, B.T. Hyman, and D.P. Corey. 1997. BNaC1 and BNaC2 constitute a new family of human neuronal sodium channels related to degenerins and epithelial sodium channels. *Proc. Natl. Acad. Sci. USA.* 94:1459–1464. https://doi.org/10.1073/pnas.94.4.1459

Garland, C.J., and K.A. Dora. 2017. EDH: Endothelium-dependent hyperpolarization and microvascular signalling. *Acta Physiol.* 219:152–161. https://doi.org/10.1111/apha.12649

Garland, C.J., and G.A. McPherson. 1992. Evidence that nitric oxide does not mediate the hyperpolarization and relaxation to acetylcholine in the rat small mesenteric artery. *Br. J. Pharmacol.* 105:429–435. https://doi.org/10.1111/j.1476-5381.1992.tb14270.x

Grifoni, S.C., N.L. Jernigan, G. Hamilton, and H.A. Drummond. 2008. ASIC proteins regulate smooth muscle cell migration. *Microvasc. Res.* 75: 202–210. https://doi.org/10.1016/j.mvr.2007.08.003

Gründer, S., H.S. Geissler, E.L. Bässler, and J.P. Ruppersberg. 2000. A new member of acid-sensing ion channels from pituitary gland. *Neuroreport.* 11:1607–1611. https://doi.org/10.1097/00001756-200006050-00003

Herbert, L.M., C.H. Nitta, T.R. Yellowhair, C. Browning, L.V. Gonzalez Bosc, T.C. Resta, and N.L. Jernigan. 2016. PICK1/calcineurin suppress ASIC1-mediated Ca^{2+} entry in rat pulmonary arterial smooth muscle cells. *Am. J. Physiol. Cell Physiol.* 310:C390–C400. https://doi.org/10.1152/ajpcell.00091.2015

Hu, Z.-L., C. Huang, H. Fu, Y. Jin, W.-N. Wu, Q.-J. Xiong, N. Xie, L.-H. Long, J.-G. Chen, and F. Wang. 2010. Disruption of PICK1 attenuates the function of ASICs and PKC regulation of ASICs. *Am. J. Physiol. Cell Physiol.* 299: C1355–C1362. https://doi.org/10.1152/ajpcell.00569.2009

Huda, R., S.L. Pollema-Mays, Z. Chang, G.F. Alheid, D.R. McCrimmon, and M. Martina. 2012. Acid-sensing ion channels contribute to chemosensitivity of breathing-related neurons of the nucleus of the solitary tract. *J. Physiol.* 590:4761–4775. https://doi.org/10.1113/jphysiol.2012.232470

Ishii, T.M., C. Silvia, B. Hirschberg, C.T. Bond, J.P. Adelman, and J. Maylie. 1997. A human intermediate conductance calcium-activated potassium channel. *Proc. Natl. Acad. Sci. USA.* 94:11651–11656. https://doi.org/10.1073/pnas.94.21.11651

Jernigan, N.L., J.S. Naik, and T.C. Resta. 2021. Acid-sensing ion channel 1 contributes to pulmonary arterial smooth muscle cell depolarization following hypoxic pulmonary hypertension. *J. Physiol.* 599:4749–4762. https://doi.org/10.1113/JP282231

Jernigan, N.L., M.L. Paffett, B.R. Walker, and T.C. Resta. 2009. ASIC1 contributes to pulmonary vascular smooth muscle store-operated Ca^{2+} entry. *Am. J. Physiol. Lung Cell. Mol. Physiol.* 297:L271–L285. https://doi.org/10.1152/ajplung.00020.2009

Kim, S., L. Ma, K.L. Jensen, M.M. Kim, C.T. Bond, J.P. Adelman, and C.R. Yu. 2012. Paradoxical contribution of SK3 and GIRK channels to the activation of mouse vomeronasal organ. *Nat. Neurosci.* 15:1236–1244. https://doi.org/10.1038/nn.3173

Köhler, M., B. Hirschberg, C.T. Bond, J.M. Kinzie, N.V. Marrion, J. Maylie, and J.P. Adelman. 1996. Small-conductance, calcium-activated potassium channels from mammalian brain. *Science.* 273:1709–1714. https://doi.org/10.1126/science.273.5282.1709

Krishnan, V., S. Ali, A.L. Gonzales, P. Thakore, C.S. Griffin, E. Yamasaki, M.G. Alvarado, M.T. Johnson, M. Trebak, and S. Earley. 2022. STIM1-dependent peripheral coupling governs the contractility of vascular smooth muscle cells. *Elife.* 11:e70278. https://doi.org/10.7554/eLife.70278

Kweon, H.-J., S.-Y. Yu, D.-I. Kim, and B.-C. Suh. 2015. Differential regulation of proton-sensitive ion channels by phospholipids: A comparative study between ASICs and TRPV1. *PLoS One.* 10:e0122014. https://doi.org/10.1371/journal.pone.0122014

Ledoux, J., A.D. Bonev, and M.T. Nelson. 2008. Ca^{2+}-activated K^+ channels in murine endothelial cells: Block by intracellular calcium and magnesium. *J. Gen. Physiol.* 131:125–135. https://doi.org/10.1085/jgp.200709875

Li, H.-S., X.-Y. Su, X.-L. Song, X. Qi, Y. Li, R.-Q. Wang, O. Maximyuk, O. Krishtal, T. Wang, H. Fang, et al. 2019. Protein kinase C lambda mediates acid-sensing ion channel 1a-dependent cortical synaptic plasticity and pain hypersensitivity. *J. Neurosci.* 39:5773–5793. https://doi.org/10.1523/JNEUROSCI.0213-19.2019

Lin, L.-H., J. Jin, M.B. Nashelsky, and W.T. Talman. 2014. Acid-sensing ion channel 1 and nitric oxide synthase are in adjacent layers in the wall of rat and human cerebral arteries. *J. Chem. Neuroanat.* 61-62:161–168. https://doi.org/10.1016/j.jchemneu.2014.10.002

Lingueglia, E., J.R. de Weille, F. Bassilana, C. Heurteaux, H. Sakai, R. Waldmann, and M. Lazdunski. 1997. A modulatory subunit of acid sensing ion channels in brain and dorsal root ganglion cells. *J. Biol. Chem.* 272: 29778–29783. https://doi.org/10.1074/jbc.272.47.29778

Liou, J., M.L. Kim, W.D. Heo, J.T. Jones, J.W. Myers, J.E. Ferrell Jr, and T. Meyer. 2005. STIM is a Ca^{2+} sensor essential for Ca^{2+}-store-depletion-triggered Ca^{2+} influx. *Curr. Biol.* 15:1235–1241. https://doi.org/10.1016/j.cub.2005.05.055

Lu, R., C. Flauaus, L. Kennel, J. Petersen, O. Drees, W. Kallenborn-Gerhardt, P. Ruth, R. Lukowski, and A. Schmidtko. 2017. $K_{Ca}3.1$ channels modulate the processing of noxious chemical stimuli in mice. *Neuropharmacology.* 125:386–395. https://doi.org/10.1016/j.neuropharm.2017.08.021

Lu, Y., X. Ma, R. Sabharwal, V. Snitsarev, D. Morgan, K. Rahmouni, H.A. Drummond, C.A. Whiteis, V. Costa, M. Price, et al. 2009. The ion channel ASIC2 is required for baroreceptor and autonomic control of the circulation. *Neuron.* 64:885–897. https://doi.org/10.1016/j.neuron.2009.11.007

Lu, Y., C.A. Whiteis, K.A. Sluka, M.W. Chapleau, and F.M. Abboud. 2013. Responses of glomus cells to hypoxia and acidosis are uncoupled, reciprocal and linked to ASIC3 expression: Selectivity of chemosensory transduction. *J. Physiol.* 591:919–932. https://doi.org/10.1113/jphysiol.2012.247189

Marra, S., R. Ferru-Clément, V. Breuil, A. Delaunay, M. Christin, V. Friend, S. Sebille, C. Cognard, T. Ferreira, C. Roux, et al. 2016. Non-acidic activation of pain-related acid-sensing Ion Channel 3 by lipids. *EMBO J.* 35: 414–428. https://doi.org/10.15252/embj.201592335

Nagao, T., S. Illiano, and P.M. Vanhoutte. 1992. Heterogeneous distribution of endothelium-dependent relaxations resistant to NG-nitro-L-arginine in rats. *Am. J. Physiol.* 263:H1090–H1094. https://doi.org/10.1152/ajpheart.1992.263.4.H1090

Naik, J.S., J.M. Osmond, B.R. Walker, and N.L. Kanagy. 2016. Hydrogen sulfide-induced vasodilation mediated by endothelial TRPV4 channels. *Am. J. Physiol. Heart Circ. Physiol.* 311:H1437–H1444. https://doi.org/10.1152/ajpheart.00465.2016

Naik, J.S., and B.R. Walker. 2018. Endothelial-dependent dilation following chronic hypoxia involves TRPV4-mediated activation of endothelial BK channels. *Pflugers Arch.* 470:633–648. https://doi.org/10.1007/s00424-018-2112-5

Nilius, B., and G. Droogmans. 2001. Ion channels and their functional role in vascular endothelium. *Physiol. Rev.* 81:1415–1459. https://doi.org/10.1152/physrev.2001.81.4.1415

Nitta, C.H., D.A. Osmond, L.M. Herbert, B.F. Beasley, T.C. Resta, B.R. Walker, and N.L. Jernigan. 2014. Role of ASIC1 in the development of chronic hypoxia-induced pulmonary hypertension. *Am. J. Physiol. Heart Circ. Physiol.* 306:H41–H52. https://doi.org/10.1152/ajpheart.00269.2013

Noureddine, A., M.L. Paffett, S. Franco, A.E. Chan, S. Pallikkuth, K. Lidke, and R.E. Serda. 2021. Endolysosomal mesoporous silica nanoparticle trafficking along microtubular highways. *Pharmaceutics.* 14:56. https://doi.org/10.3390/pharmaceutics14010056

Ottolini, M., Z. Daneva, Y.-L. Chen, E.L. Cope, R.B. Kasetti, G.S. Zode, and S.K. Sonkusare. 2020. Mechanisms underlying selective coupling of endothelial Ca^{2+} signals with eNOS vs. Ik/SK channels in systemic and

pulmonary arteries. *J. Physiol.* 598:3577–3596. https://doi.org/10.1113/JP279570

Paffett, M.L., J.S. Naik, T.C. Resta, and B.R. Walker. 2007. Reduced store-operated Ca^{2+} entry in pulmonary endothelial cells from chronically hypoxic rats. *Am. J. Physiol. Lung Cell. Mol. Physiol.* 293:L1135–L1142. https://doi.org/10.1152/ajplung.00432.2006

Petroff, E., V. Snitsarev, H. Gong, and F.M. Abboud. 2012. Acid sensing ion channels regulate neuronal excitability by inhibiting BK potassium channels. *Biochem. Biophys. Res. Commun.* 426:511–515. https://doi.org/10.1016/j.bbrc.2012.08.114

Petroff, E.Y., M.P. Price, V. Snitsarev, H. Gong, V. Korovkina, F.M. Abboud, and M.J. Welsh. 2008. Acid-sensing ion channels interact with and inhibit BK K^+ channels. *Proc. Natl. Acad. Sci. USA.* 105:3140–3144. https://doi.org/10.1073/pnas.0712280105

Price, M.P., P.M. Snyder, and M.J. Welsh. 1996. Cloning and expression of a novel human brain Na^+ channel. *J. Biol. Chem.* 271:7879–7882. https://doi.org/10.1074/jbc.271.14.7879

Qiu, F., C.-Y. Qiu, Y.-Q. Liu, D. Wu, J.-D. Li, and W.-P. Hu. 2012. Potentiation of acid-sensing ion channel activity by the activation of 5-HT_2 receptors in rat dorsal root ganglion neurons. *Neuropharmacology*. 63:494–500. https://doi.org/10.1016/j.neuropharm.2012.04.034

Redd, M.A., S.E. Scheuer, N.J. Saez, Y. Yoshikawa, H.S. Chiu, L. Gao, M. Hicks, J.E. Villanueva, Y. Joshi, C.Y. Chow, et al. 2021. Therapeutic inhibition of acid-sensing ion channel 1a recovers heart function after ischemia-reperfusion injury. *Circulation*. 144:947–960. https://doi.org/10.1161/CIRCULATIONAHA.121.054360

Ren, C., X. Gan, J. Wu, C.-Y. Qiu, and W.-P. Hu. 2016. Enhancement of acid-sensing ion channel activity by metabotropic P2Y UTP receptors in primary sensory neurons. *Purinergic Signal.* 12:69–78. https://doi.org/10.1007/s11302-015-9479-y

Roos, J., P.J. DiGregorio, A.V. Yeromin, K. Ohlsen, M. Lioudyno, S. Zhang, O. Safrina, J.A. Kozak, S.L. Wagner, M.D. Cahalan, et al. 2005. STIM1, an essential and conserved component of store-operated Ca^{2+} channel function. *J. Cell Biol.* 169:435–445. https://doi.org/10.1083/jcb.200502019

Schaefer, L., H. Sakai, M. Mattei, M. Lazdunski, and E. Lingueglia. 2000. Molecular cloning, functional expression and chromosomal localization of an amiloride-sensitive Na^+ channel from human small intestine. *FEBS Lett.* 471:205–210. https://doi.org/10.1016/S0014-5793(00)01403-4

Shimokawa, H., H. Yasutake, K. Fujii, M.K. Owada, R. Nakaike, Y. Fukumoto, T. Takayanagi, T. Nagao, K. Egashira, M. Fujishima, and A. Takeshita. 1996. The importance of the hyperpolarizing mechanism increases as the vessel size decreases in endothelium-dependent relaxations in rat mesenteric circulation. *J. Cardiovasc. Pharmacol.* 28:703–711. https://doi.org/10.1097/00005344-199611000-00014

Smith, E.S., H. Cadiou, and P.A. McNaughton. 2007. Arachidonic acid potentiates acid-sensing ion channels in rat sensory neurons by a direct action. *Neuroscience*. 145:686–698. https://doi.org/10.1016/j.neuroscience.2006.12.024

Song, N., R. Guan, Q. Jiang, C.J. Hassanzadeh, Y. Chu, X. Zhao, X. Wang, D. Yang, Q. Du, X.-P. Chu, and L. Shen. 2016. Acid-sensing ion channels are expressed in the ventrolateral medulla and contribute to central chemoreception. *Sci. Rep.* 6:38777. https://doi.org/10.1038/srep38777

Sonkusare, S.K., A.D. Bonev, J. Ledoux, W. Liedtke, M.I. Kotlikoff, T.J. Heppner, D.C. Hill-Eubanks, and M.T. Nelson. 2012. Elementary Ca^{2+} signals through endothelial TRPV4 channels regulate vascular function. *Science*. 336:597–601. https://doi.org/10.1126/science.1216283

Suh, B.-C., and B. Hille. 2008. PIP2 is a necessary cofactor for ion channel function: How and why? *Annu. Rev. Biophys.* 37:175–195. https://doi.org/10.1146/annurev.biophys.37.032807.125859

Tan, Z.-Y., Y. Lu, C.A. Whiteis, A.E. Simms, J.F.R. Paton, M.W. Chapleau, and F.M. Abboud. 2010. Chemoreceptor hypersensitivity, sympathetic excitation, and overexpression of ASIC and TASK channels before the onset of hypertension in SHR. *Circ. Res.* 106:536–545. https://doi.org/10.1161/CIRCRESAHA.109.206946

Waldmann, R., F. Bassilana, J. de Weille, G. Champigny, C. Heurteaux, and M. Lazdunski. 1997a. Molecular cloning of a non-inactivating proton-gated Na^+ channel specific for sensory neurons. *J. Biol. Chem.* 272:20975–20978. https://doi.org/10.1074/jbc.272.34.20975

Waldmann, R., G. Champigny, F. Bassilana, C. Heurteaux, and M. Lazdunski. 1997b. A proton-gated cation channel involved in acid-sensing. *Nature*. 386:173–177. https://doi.org/10.1038/386173a0

Wang, Y.-C., W.-Z. Li, Y. Wu, Y.-Y. Yin, L.-Y. Dong, Z.-W. Chen, and W.-N. Wu. 2015. Acid-sensing ion channel 1a contributes to the effect of extracellular acidosis on NLRP1 inflammasome activation in cortical neurons. *J. Neuroinflammation*. 12:246. https://doi.org/10.1186/s12974-015-0465-7

Wemmie, J.A., J. Chen, C.C. Askwith, A.M. Hruska-Hageman, M.P. Price, B.C. Nolan, P.G. Yoder, E. Lamani, T. Hoshi, J.H. Freeman Jr, and M.J. Welsh. 2002. The acid-activated ion channel ASIC contributes to synaptic plasticity, learning, and memory. *Neuron*. 34:463–477. https://doi.org/10.1016/S0896-6273(02)00661-X

Xia, X.-M., B. Fakler, A. Rivard, G. Wayman, T. Johnson-Pais, J.E. Keen, T. Ishii, B. Hirschberg, C.T. Bond, S. Lutsenko, et al. 1998. Mechanism of calcium gating in small-conductance calcium-activated potassium channels. *Nature*. 395:503–507. https://doi.org/10.1038/26758

Xiong, Z., Y. Liu, L. Hu, B. Ma, Y. Ai, and C. Xiong. 2013. A rapid facilitation of acid-sensing ion channels current by corticosterone in cultured hippocampal neurons. *Neurochem. Res.* 38:1446–1453. https://doi.org/10.1007/s11064-013-1045-9

Xiong, Z.G., X.M. Zhu, X.P. Chu, M. Minami, J. Hey, W.L. Wei, J.F. MacDonald, J.A. Wemmie, M.P. Price, M.J. Welsh, and R.P. Simon. 2004. Neuroprotection in ischemia: Blocking calcium-permeable acid-sensing ion channels. *Cell*. 118:687–698. https://doi.org/10.1016/j.cell.2004.08.026

Yermolaieva, O., A.S. Leonard, M.K. Schnizler, F.M. Abboud, and M.J. Welsh. 2004. Extracellular acidosis increases neuronal cell calcium by activating acid-sensing ion channel 1a. *Proc. Natl. Acad. Sci. USA.* 101:6752–6757. https://doi.org/10.1073/pnas.0308636100

Zhang, D.X., K.M. Gauthier, Y. Chawengsub, and W.B. Campbell. 2007. ACh-induced relaxations of rabbit small mesenteric arteries: Role of arachidonic acid metabolites and K^+. *Am. J. Physiol. Heart Circ. Physiol.* 293:H152–H159. https://doi.org/10.1152/ajpheart.00268.2006

Zhang, L., T.-D. Leng, T. Yang, J. Li, and Z.-G. Xiong. 2020. Protein kinase C regulates ASIC1a protein expression and channel function via NF-kB signaling pathway. *Mol. Neurobiol.* 57:4754–4766. https://doi.org/10.1007/s12035-020-02056-4